branch, Tokyo. She wore the template there on August 6, 2011 during her summer-time holiday, as previously reported (1). She used the template during sleeping and 2 h exercise for over 3 months. Her symptoms such as non-specific complaints, had disappeared after a week. Whole saliva (2-5 ml) was collected in a 50 ml centrifugation tube and immediately frozen at –20°C six times at 15, 14, 12, 10, 8, 4 days before the therapy and six times at 1, 3, 8, 14, 18, 22 days after the therapy. The CE-TOF-MS analysis of the collected saliva has been performed, according to the Guideline of the Intramural Ethics Committee (approved as no. A1113), as described below.

Sample preparation. Saliva was thawed and centrifugally-filtered through a 5-kDa cut-off filter (Millipore, Bedford, MA, USA) at 9,100 ×*g* for at least 2.5 h at 4°C to remove macromolecules. Five microliters of Milli-Q water containing internal standards (2 mmol/l each of methionine sulfone, 2-[*N*-morpholino]-ethanesulfonic acid, D-camphor-10-sulfonic acid, 3-aminopyrrolidine, and trimesate) was added to 45 μl of the filtrate and mixed immediately before CE-TOF-MS analysis.

CE-TOF-MS analysis. The instrumentation and measurement conditions used for CE-TOF-MS are described elsewhere (12, 13) with slight modifications. Briefly, cation analysis was performed using an Agilent CE capillary electrophoresis system, an Agilent G6220A LC/MSD TOF system, an Agilent 1100 series isocratic HPLC pump, a G1603A Agilent CE-MS adapter kit, and a G1607A Agilent CE-ESI-MS sprayer kit (Agilent Technologies, Waldbronn, Germany). Anion analysis was performed using an Agilent CE capillary electrophoresis system, an Agilent G6210A LC/MSD TOF system, an Agilent 1200 series isocratic HPLC pump, a G1603A Agilent CE-MS adapter kit, and a G1607A Agilent CE-electrospray ionization (ESI) source-MS sprayer kit (Agilent Technologies). For the cation and anion analyses, the CE-MS adapter kit includes a capillary cassette that facilitates thermostatic control of the capillary. The CE-ESI-MS sprayer kit simplifies coupling of the CE system with the MS system, and is equipped with an electrospray source. For system control and data acquisition, we used G2201AA Agilent ChemStation software for CE and the Agilent MassHunter software for TOF-MS. The original Agilent SST316Ti stainless steel ESI needle was replaced with a passivated SST316Ti stainless steel and platinum needle (passivated with 1% formic acid and 20% aqueous solution of isopropanol at 80°C for 30 min) for anion analysis.

For cationic metabolite analysis using CE-TOF-MS (12), sample separation was performed in fused silica capillaries (50 μm i.d. × 100 cm total length) filled with 1 mol/l formic acid as the reference electrolyte. Sample solutions (3 nl) were injected at 50 mbar for 5 s and a voltage of 30 kV was applied. The capillary temperature was maintained at 20°C and the temperature of the sample tray was kept below 5°C. The sheath liquid, composed of methanol/water (50% v/v) and 0.1 μmol/l hexakis(2,2-difluoroethoxy) phosphazene (Hexakis), was delivered at 10 μl/min. ESI-TOF-MS was conducted in the positive ion mode. The capillary voltage was set at 4 kV and the flow rate of nitrogen gas (heater temperature=300°C) was set at 7 psig. In TOF-MS, the fragmentor, skimmer and OCT RF voltages were 75, 50 and 125 V, respectively. Automatic recalibration of each acquired spectrum was performed using reference standards {[^{13}C isotopic ion of protonated methanol dimer (2MeOH+H)]$^+$, *m/z* 66.0632)} and {[protonated Hexakis (M+H)]$^+$, *m/z* 622.0290]}. Mass spectra were acquired at the rate of 1.5 cycles/s over a *m/z* range of 50-1,000.

For anionic metabolite analysis using CE-TOF-MS (14), a commercially available COSMO(+) capillary (50 μm i.d. × 105 cm, Nacalai Tesque, Kyoto, Japan), chemically-coated with a cationic polymer, was used for separation. Ammonium acetate solution (50 mmol/l; pH 8.5) was used as the electrolyte for separation. Before the first use, the new capillary was flushed successively with the running electrolyte (pH 8.5), 50 mmol/l acetic acid (pH 3.4), and then the electrolyte again for 10 min each. Before each injection, the capillary was equilibrated for 2 min by flushing with 50 mM acetic acid (pH 3.4) and then flushed for 5 min with the running electrolyte. A sample solution (30 nl) was injected at 50 mbar for 30 s, and a voltage of –30 kV was applied. The capillary temperature was maintained at 20°C and the sample tray was cooled below 5°C. An Agilent 1100 series pump, equipped with a 1:100 splitter was used to deliver 10 μl/min of 5 mM ammonium acetate in 50% (v/v) methanol/water, containing 0.1 μM Hexakis, to the CE interface. Here, it was used as a sheath liquid surrounding the CE capillary to provide a stable electrical connection between the tip of the capillary and the grounded electrospray needle. ESI-TOF-MS was conducted in the negative ionization mode at a capillary voltage of 3.5 kV. For TOF-MS, the fragmentor, skimmer and OCT RF voltages were set at 100, 50 and 200 V, respectively. The flow rate of the drying nitrogen gas (heater temperature=300°C) was maintained at 7 psig. Automatic recalibration of each acquired spectrum was performed using reference standards {[^{13}C isotopic ion of de-protonated acetic acid dimer (2 CH_3COOH-H)]$^-$, *m/z* 120.03841}, and {[Hexakis+ deprotonated acetic acid (M+CH_3COOH-H)]$^-$, *m/z* 680.03554}. Exact mass data were acquired at a rate of 1.5 spectra/s over a *m/z* range of 50-1,000.

Data analysis and statistical analysis. Raw data were analyzed by our proprietary software MasterHands (13), which follows typical data processing flows including detecting all possible peaks, eliminating noise and redundant features, and generating the aligned data matrix with annotated metabolite identities and relative area (peak areas normalized by those of internal standards) (15). Concentrations were calculated using external standards based on relative area. To eliminate the variation of overall concentration, the concentration of each metabolite was divided by the concentration of total metabolites (relative concentration), or that of each amino acid was divided by the concentration of total amino acids. Only the metabolites frequently observed in four, or more, out of six samples before or after template therapy were used for the data analysis. The student's *t*-test (two-tailed) was used for statistical comparisons.

Results

In total, 113 substances were identified in the saliva and, out of these, 56 metabolites frequently observed were used for the data analysis. Glycine was the most abundant amino acid in the saliva, followed by proline, alanine and serine (Figure 1A). After the start of the template therapy, the patient's headache was alleviated, accompanied by significant (p=0.042) increase of the salivary concentration of glycine, as compared with total amino acids whereas that of other amino acids was not significantly changed (Figure 1B).

After template therapy, the concentration of only six metabolites was increased [fold-change (FC) >1.2), out of which priopinate and urea were the most dominant, and the

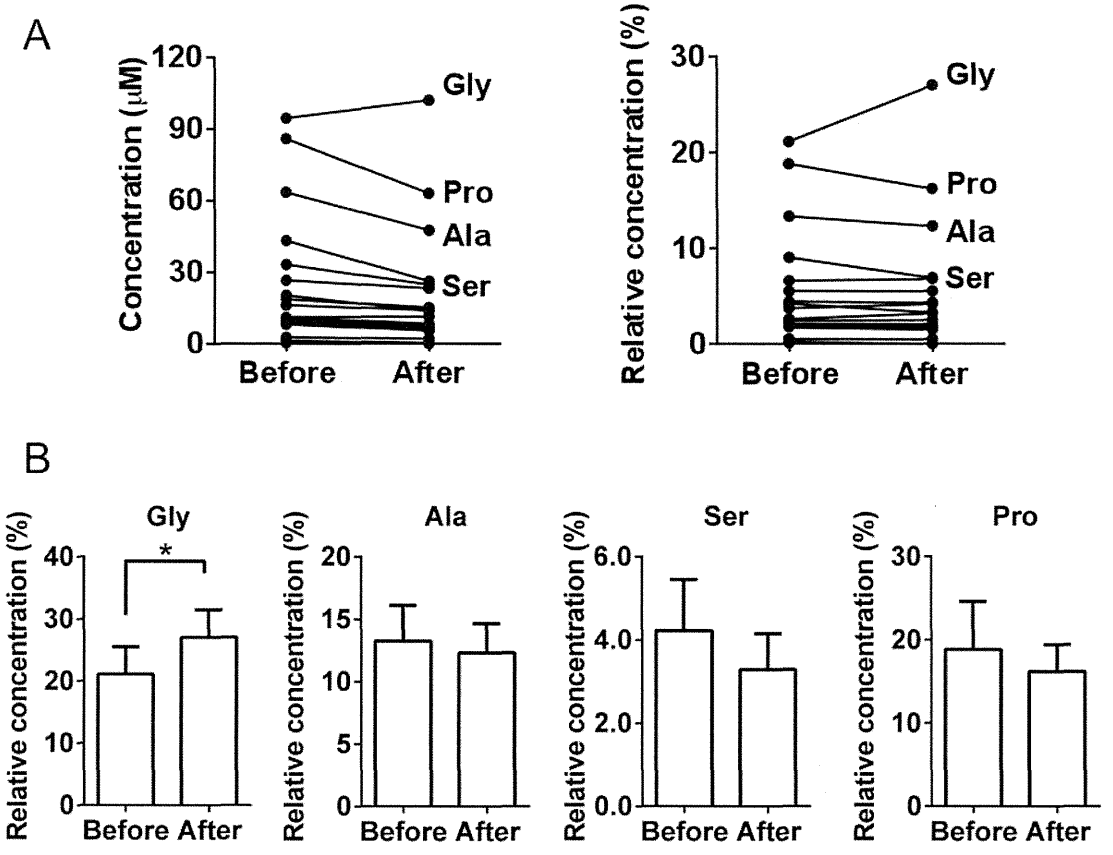

Figure 1. *Salivary amino acid concentrations before and after template therapy. A: Absolute concentration (left) and ratio of each amino acid to total amino acids (relative concentration) (right). B: Bar graph showing mean and standard deviation of the relative concentration of four major salivary amino acids, glycine, proline, alanine and serine. *p<0.05.*

relative concentrations of other metabolites were less than 1% (Figure 2A). No metabolite significantly increased in concentration. The concentration of many metabolites decreased after the therapy (FC<0.7), where *N*-acetylneuraminate (p=0.025) and *p*-hydroxyphenylacetate (p=0.039) was presented significantly decreased (Figure 2B). Out of these, 11 amino acids, namely proline, alanine, glutamate, glutamine, serine, asparagine, valine, phenylalanine, leucine, threonine and isoleucine, tended to decrease although not significantly. The other 23 metabolites, such as lactate and pyruvate, were hardly changed (data not shown).

Discussion

There are numerous reports that investigated the salivary concentration of amino acids in relation to caries (16, 17), periodontal diseases (18-20), phenylketonuria (21), migraine (22), a lacto-ovo vegetarian diet (23), smoking and gender difference (24), diurinal changes and aging (25). However, to our knowledge, none of these reports, except for ours (26), has attributed attention to the salivary glycine level. We reported that (i) glycine was the most abundant amino acid in the saliva; (ii) glycine and lysine concentrations increased significantly (p<0.05) with aging, regardless of gender difference; and (iii) glycine and lysine were positively correlated (p<0.001), (iv) however, there was no significant correlation between the salivary concentration of glutamic acid or histidine and age, suggesting that salivary amino acid levels may be regarded as markers of aging (26). The present study demonstrated that glycine was also the most abundant amino acid in the saliva of the female patient presented here, and glycine is the only amino acid that increased significantly with template therapy (Figure 1). This does not necessarily mean that the elevation of glycine is the result of accelerating the aging process, since the observed glycine concentration (at most 100 μM) is much smaller than the value reported in aged people (570 μM) (26). It is interesting to note that the plasma concentration of glycine is significantly reduced by occlusal destruction, producing the opposite effect to template therapy (27).

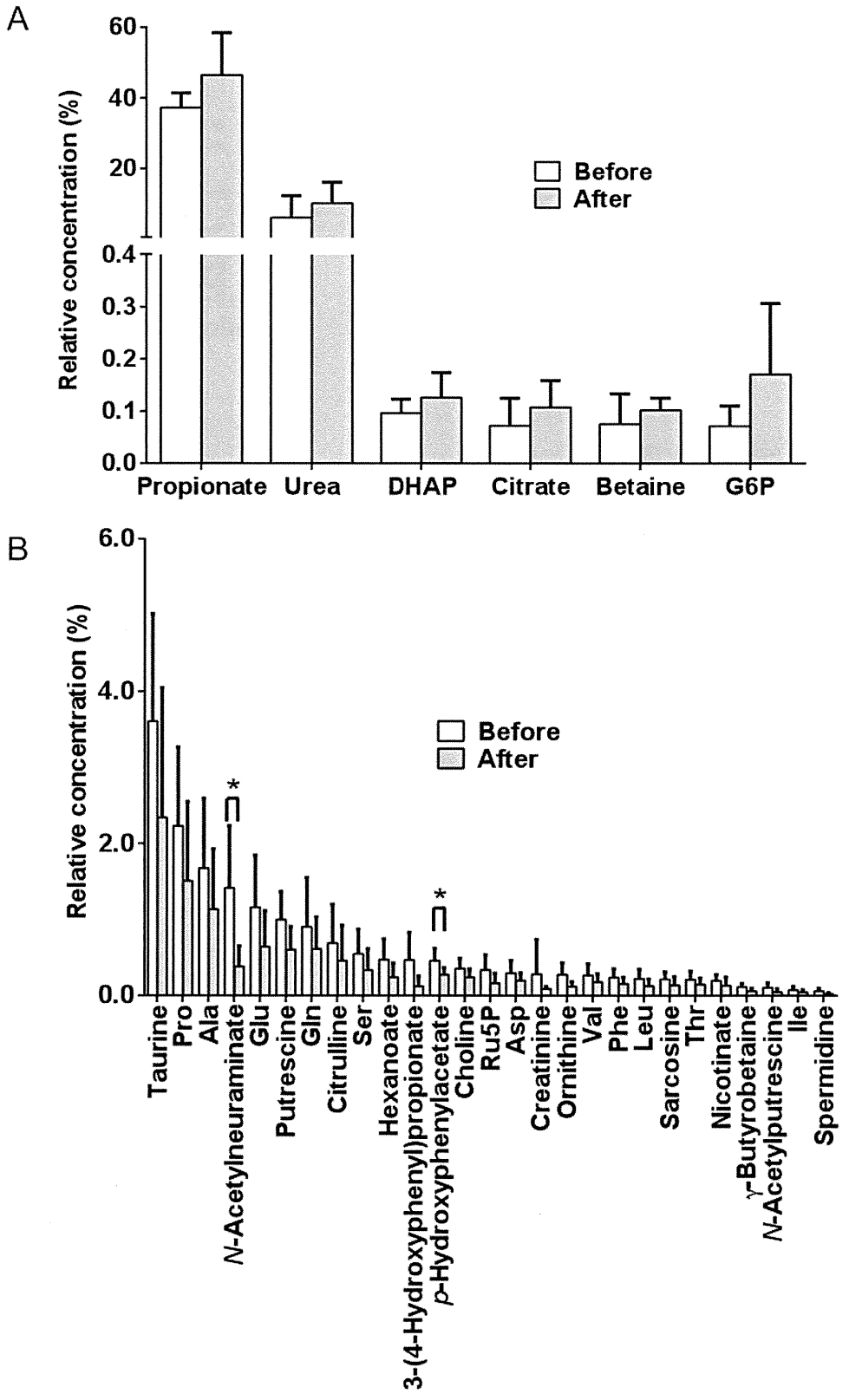

Figure 2. *Relative concentrations of metabolites before and after the template therapy. Metabolites increased (fold-change (FC) >1.2) (A) and reduced (FC<0.7) (B) after template therapy. Bar graph indicates mean and standard deviation. *p<0.05.*

The biological significance of the increase of the relative concentration of glycine by template therapy is unclear. Recent reports have suggested the possible role of glycine in inflammation. Glycine stimulated production of pro-inflammatory substances such as nitric oxide, prostaglandin E_2, tumor necrosis factor-α and cyclooxygenase-2 in macrophages, gingival fibroblasts and microglia (28-30). On the other hand, glycine exerts anti-inflammatory activity *via* glycine-activated chloride channels that suppress the production of oxidants and pro-inflammatory cytokines (31) and protected the cells from cadmium (32), cyclosporine-induced kidney damage (33) and liver injury (34, 35), suggesting a possible role of glycine in cell survival and activation. These data suggest dual actions of glycine.

In the metabolomics profiles, a large number of metabolites decreased in concentration (n=27) while that of a few metabolites increased (n=6) on template therapy. The decreased metabolites included many compounds related to nervous systems status; taurine was the most abundant and this metabolite acts as an inhibitory neurotransmitter and is used to aid the treatment of epilepsy and excitable brain status (36). Glutamine and asparagine are excitatory neurotransmitters within the central nervous system responsible for normal synaptic neurotransmission, serine acts as both neurotransmitter and neuromodulator, and alanine is also a neurotransmitter in the visual system (36). Only *N*-acetylneuraminate and *p*-phydroxyphenylacetate showed significant reduction (p=0.025 and p=0.039, respectively) after template therapy. *N*-Acetylneuraminate is the most prominent sialic acid that is a terminal sugar and acts as a marker for chronic inflammation in various systemic diseases, such as heart diseases (37, 38) and breast cancer (39). *p*-Hydroxyphenylacetate is expected to be produced by oral bacteria (40). Thus, the significant decrease of these salivary components might reflect the metabolic change of both systemic and oral physiological conditions. Further extensive studies with more patients are required to elucidate the biological significance of the present findings.

Acknowledgements

This work was supported by research funds from the Yamagata Prefectural Government and the City of Tsuruoka, and in part by a Grant-in-Aid for Scientific Research (C) of the Ministry of Education, Culture, Sports, Science and Technology of Japan (S. Tanaka, no. 24593164).

References

1 Maehara K, Tsuruhara T, Hase Y, Fukuda Y, Sawada Y, Yamamoto Y, Nakamura S, Takesada M, Nakajima A, Ito H, Matsui T, Takada F, Ueda T, Guzay C and Sato S: A template therapy approach for non-specific complaints. Basal Facts *8*: 22-35, 1986.

2 Nobili A and Adversi R: Relationship between posture and occlusion; A clinical and experimental investigation. J Craniomandib Pract *14*: 274-285, 1996.

3 Milani RS, de Periere DD and Micallef J-P: Relationship between dental occlusion and visual focusing. J Craniomandib Pract *16*: 109-118, 1998.

4 Tokita K, Ito R, Kawamura H, Sato Y, Terada K, Yamada M and Henomatsu H: Studies on teeth extraction phenomena. Comparative studies on electrocardiographic and histologic findings in rats, mice, hamsters and guinea-pigs. J Am College Cardiol *24*: 975-976, 1960.

5 Abe K, Yokota Y, Kawazoe T, Hioki S, Kishimoto T and Dawes C: The effects of an incisal bite plane on rat submandibular gland. J Dent Res *62*: 721-724, 1983.

6 Hioki S, Niwa K, Kishimoto T, Kawazoe T, Yokota Y, Abe K and Dawes C: The effects of an incisal bite plane on rat sublingual glands. J Dent Res *62*: 715-721, 1983.

7 Ueda T: Effects of occlusal destruction on posture in rats. J Gifu Dent Soc *18*: 192-202, 1991 (in Japanese).

8 Sumioka T: Systemic effects of the peripheral disturbance of the trigeminal system. Influence of the occlusal destruction in dogs. J Kyoto Pref Univ Med *98*: 1077-1085, 1991.

9 Azuma Y, Maehara K, Tokunaga T, Hashimoto M, Ieoka K and Sakagami H: Systemic effects of the occlusal destruction in guinea pigs. In Vivo *13*: 519-524, 1999.

10 Taga H, Azuma Y, Maehara K and Nomura S: Effects of changes in occlusal vertical dimension on heart rate fluctuations in guinea pigs. In Vivo *28*: 177-182, 2012

11 Soga T, Baran R, Suematsu M, Ueno Y, Ikeda S, Sakurakawa T, Kakazu Y, Ishikawa T, Robert M, Nishioka T and Tomita M: Differential metabolomics reveals ophthalmic acid as an oxidative stress biomarker indicating hepatic glutathione consumption. J Biol Chem *281*: 16768-16776, 2006.

12 Sugimoto M, Wong DT, Hirayama A, Soga T and Tomita M: Capillary electrophoresis mass spectrometry-based saliva metabolomics identified oral, breast and pancreatic cancer-specific profiles. Metabolomics *6*: 78-95, 2010.

13 Soga T, Igarashi K, Ito C, Mizobuchi K, Zimmermann HP and Tomita M: Metabolomic profiling of anionic metabolites by capillary electrophoresis mass spectrometry. Analytical chemistry *81*: 6165-6174, 2009.

14 Sugimoto M, Kawakami M, Robert M, Soga T and Tomita M: Bioinformatics tools for mass spectroscopy-based metabolomic data processing and analysis. Curr Bioinform *7*: 96-108, 2012.

15 Van Wuyckhuyse BC, Perinpanayagam HER, Bevacqua D, Raubertas RFm Billings RJ, Bowen WH and Tabak LA: Association of free arginine and lysine concentrations in human parotid saliva with caries experience. J Dent Res *74*: 686-690, 1995.

16 Fonteles CSR, Guerra MH, Ribeiro TR, Mendonça DN, de Carualho CBM, Monteiro AJ, Toyama DO, Toyama MH and Fonteles MC: Association of free amino acids with caries experience and *mutans streptococci* levels in whole saliva of children with early childhood caries. Arch Oral Biol *54*: 80-85, 2009.

17 Syrjänen S, Piironen P and Markkanen H: Free amino acid composition of wax-stimulated whole saliva in human subjects with healthy periodontium, severe chronic periodontitis and post-juvenile periodontitis. Arch Oral Biol *29*: 735-738, 1984.

18 Syrjänen S, Piironen P and Markkanen H: Free amino acid content of wax-stimulated human whole saliva as related to periodontal disease. Arch Oral Biol *32*: 607-610, 1987.

19 Syrjänen SM, Alakuijala P, Markkanen SO and Markkanen H: Free amino acid levels in oral fluids of normal subjects and patients with periodontal disease. Arch Oral Biol *35*: 189-193, 1990.
20 Liappis N, Pohl B, Weber HP and el-Karkani H: Free amino acids in saliva of children with phenylketonuria. Klin Padiatr *198*: 25-28,1986.
21 Rajda C, Tajti J, Komoróczy R, Seres E, Klivényi P and Vécsei L: Amino acids in the saliva of patients with migraine. Headache *39*: 644-649, 1999.
22 Linkosalo E, Markkanen H and Syrjanen S: Effects of a lacto-ovo vegetarian diet on the free amino acid composition of wax-stimulated whole human saliva. J Nutr *115*: 588-592, 1985.
23 Takeda I, Stretch C, Barnaby P, Bhatnager K, Rankin K, Fu H, Weljie A, Jha N and Slupsky C: Understanding the human salivary metabolome. NMR Biomed *22*: 577-584, 2009.
24 Bertram HC, Eggers N and Eller N: Potential of human saliva for nuclear magnetic resonance-based metabolomics and for health-related biomarker identification. Anal Chem *81*: 9188-9193, 2009.
25 Tanaka S, Machino M, Akita S, Yokote Y and Sakagami H: Changes in salivary amino acid composition during aging. In Vivo *24*: 853-856, 2010.
26 Maehara K, Taga H, Takayama F and Sakagami H: Biochemical Analysis of Occlusal Destruction. 48th Japanese Association for Oral Biology, Tsurumi, Kanagawa, Japan, 2006 abstract poster no. 374.
27 Carmans S, Hendriks JJ, Thewissen K, Van den Eynden J, Stinissen P, Rigo JM and Hellings N: The inhibitory neurotransmitter glycine modulates macrophage activity by activation of neutral amino acid transporters. J Neurosci Res *88*: 2420-2430, 2010.
28 Rausch-Fan X, Ulm C, Jensen-Jarolim E, Shcedle A, Boltz-Nitulescu G, Rausch WD and Matejka M: Interleukin-1β-induced prostaglandin E2 production by human gingival fibroblasts is up-regulated by glycine. J Periodontol *76*: 1182-1188, 2005.
29 Tanaka J, Toku K, Matsuda S, Sudo S, Fujita H, Sakanaka M and Maeda N: Induction of resting microglia in culture medium devoid of glycine and serine. Glia *24*: 198-215, 1998.
30 McCarty MF, Barroso-Aranda J and Contreras F: The hyperpolarizing impact of glycine on endothelial cells may be anti-atherogenic. Med Hypotheses *73*: 263-264, 2009.
31 Okoto T and Awhin EP: Glycine reduces cadmium-induced alterations in the viability and activation of macrophage U937 cells. Food Chem Toxicol *48*: 536-538, 2010.
32 Thurman RG, Zhong Z, von Frankenberg M, Stachlewitz RF and Bunzendahl H: Prevention of cyclosporine-induced nephrotoxicity with dietary glycine. Transplantation *63*: 1661-1667, 1997.
33 Benko T, Freda S, Gu Y, Best J, Baba HA, Schlaak JF, de Groot H, Fandrey J and Rauen U: Glycine pretreatment ameliorates liver injury after partial hepatectomy in the rat. J Invest Surg *23*: 12-20, 2010.
34 You HB, Wang Q, Li XH, Chen XF, Liu Zj and Gong JP: The protection mechanisms of glycine against liver injury induced by lipopolysaccharides. Zhonghua Gan Zang Bing Za Zhi *14*: 574-577, 2006 (in Chinese).
35 Zinellu A, Sotgia S, Pisanu E, Scanu B, Sanna M, Usai MF, Chessa R, Deiana L and Carru C: Quantification of neurotransmitter amino acids by capillary electrophoresis laser-induced fluorescence detection in biological fluids. Anal Bioanal Chem *398*: 1973-1978, 2010.
36 Hegde AM, Kavita R, Sushma KS and Suchetha S: Salivary sialic acid levels and dental health in children with congenital heart disease. J Clin Pediatr Dent *36*: 293-296, 2012.
37 Oktay S, Basar I, Emekli-Alturfan E, Malali E, Elemek E, Ayan F, Koldas L, Noyan U and Emekli N: Serum and saliva sialic acid in periodontitis patients with and without cardiovascular disease. Pathophysiol Haemost Thromb *37*: 67-71, 2010.
38 Ozturk LK, Emekli-Alturfan E, Kasikci E, Demir G and Yarat A: Salivary total sialic acid levels increase in breast cancer patients: A preliminary study. Med Chem *7*: 443-447, 2011.
39 O'Connor KE, Witholt B and Duetz W: p-Hydroxyphenylacetic acid metabolism in Pseudomonas putida F6. J Bacteriol *183*: 928-933, 2001.

Received September 10, 2012
Revised October 16, 2012
Accepted October 17, 2012

Analyst

Cite this: *Analyst*, 2012, **137**, 5026

www.rsc.org/analyst

PAPER

Sheathless capillary electrophoresis-mass spectrometry with a high-sensitivity porous sprayer for cationic metabolome analysis

Akiyoshi Hirayama, Masaru Tomita and Tomoyoshi Soga*

Received 12th April 2012, Accepted 8th September 2012
DOI: 10.1039/c2an35492f

Sheath-flow capillary electrophoresis-mass spectrometry (CE-MS) has emerged as a new tool for comprehensive analysis of charged metabolites. However, it needs to be more sensitive. Here, we report a sheathless capillary electrophoresis-electrospray ionization-mass spectrometry method for cationic metabolome analysis. This system used a high-sensitivity porous sprayer interface and 10% (v/v) acetic acid as the background electrolyte (BGE). Under optimized conditions, 53 cationic metabolites, including amino acids and their derivatives, amines, nucleic acids and small peptides, were successfully separated and selectively detected with a time-of-flight mass spectrometer. At a signal-to-noise ratio of three, the concentration detection limits for these compounds were between 0.004 and 0.8 μmol L^{-1} (amount detection limit, 0.01 to 2 fmol) with pressure injection at 20.7 kPa for 5 s (2.6 nL). Compared with conventional sheath-flow CE-MS, the detection limit of the present method was increased more than 5-fold for 21 (40%) of the compounds detected. When the method was applied to the analysis of cationic metabolites obtained from human urine, there was a 10-fold increase in the number of detected peaks compared with conventional methods. More than 180 successive runs could be conducted without any problems, and only the BGE needed to be changed.

Introduction

Metabolomics is the comprehensive analysis of endogenous small molecule metabolites (typically less than 1 kDa) in biological samples. Gas chromatography/mass spectrometry,[1,2] liquid chromatography-mass spectrometry,[3] or nuclear magnetic resonance spectroscopy[4] are commonly used for metabolomics. However, a standard metabolomics method has not been established. This is primarily because of the complexity, chemical diversity, and physical properties of the metabolome.[5] Recently, we have developed capillary electrophoresis-mass spectrometry (CE-MS) for metabolome analysis and successfully analyzed thousands of charged metabolites simultaneously.[6–12] The major advantages of CE-MS are its extremely high resolution, and that almost any charged species can be infused into the mass spectrometer.

Electrospray ionization (ESI) is a soft ionization technique that is suitable for mass measurement of species over a broad molecular mass range. ESI is commonly used for liquid chromatography-mass spectrometry and CE-MS analysis. However, in sheath-flow CE-MS, the ESI sprayer needs a sheath liquid to establish an electrical contact between the ends of the capillary and maintain stable electrospray. However, the main disadvantage of sheath-flow configurations is their low sensitivity because of dilution of the analyte by the sheath liquid.[13]

To improve sensitivity, various sheathless CE-MS interfaces have been developed. For example, the outer surface of the capillary has been coated with conductive materials such as gold,[14,15] silver,[16] copper,[17] or graphite,[18] which allow the electrical contact to be established. However, these coatings are often damaged by electrical discharge and this reduces the lifetime of the electrical contact. In another approach, a platinum wire was inserted into the capillary to establish a stable electric contact,[19] but this caused bubble formation in the capillary. A split-flow technique has been developed where a small hole or a locally porous section was made near the capillary outlet wall, and a small portion of the background electrolyte (BGE) exited through this hole/section and contacted with an external electrode *via* the BGE reservoir.[20,21] However, most of these techniques require special equipment and skilled operators, which limits their application.

Recently, Moini has introduced a novel sheathless interface consisting of a porous tip at the capillary, and the electrical connection was established through this tip.[22] To form the porous tip, a 3–4 cm section of the capillary outlet was etched with a solution of 49% hydrofluoric acid. The electrical contact between the porous capillary and the ESI was achieved by filling the ESI needle with a static conductive liquid.

Based on this concept, a prototype high-sensitivity porous sprayer (HSPS) sheathless interface for CE-MS has been recently

Institute for Advanced Biosciences, Keio University, Tsuruoka, Yamagata 997-0052, Japan. E-mail: soga@sfc.keio.ac.jp; Fax: +81-235-29-0574; Tel: +81-235-29-0528

developed by Beckman Coulter (Brea, CA). This HSPS has been used for the analysis of peptide mixtures,[23,24] intact proteins,[25] and phosphorus-containing amino acid-type herbicides.[26] Recently, Ramautar *et al.* have evaluated the performance of this interface for the analysis of 21 metabolites including amino acids and their derivatives in urine sample.[27] Nevertheless, the evaluation of HSPS sheathless interface on other physiologically important metabolites has yet to be demonstrated.

In this study, we developed a sheathless CE-MS method using the prototype HSPS capillary to analyze a wider range of cationic metabolites. We have selected 53 metabolites including amino acids and their derivatives, amines, nucleic acids and small peptides, which are metabolically important intermediates in amino acid anabolism/catabolism, purine/pyrimidine metabolism and glutathione biosynthesis, and therefore important for the understanding of the global metabolism in living systems. The sensitivities from the optimized method were compared with those from conventional sheath-flow CE-MS, and the developed method was applied to metabolome analysis of human urine.

Results and discussion

Development of sheathless CE-MS using a HSPS capillary

In sheathless CE-MS, the BGE composition and pH are important factors for controlling the peak resolution because these parameters affect the electroosmotic flow rate. We first tried 1 mol L^{-1} formic acid (pH 1.8) as the BGE, because it is often used in conventional sheath-flow CE-MS.[28] However, with formic acid, the current dropped several minutes after applying voltage, although the reason for this was unclear. To overcome this problem, we examined alternative BGEs and found that the drop in current did not occur with acetic acid. The effect of changing the acetic acid concentration (100 mmol L^{-1}, 850 mmol L^{-1}, and 1.7 mol L^{-1}) on the resolution of leucine and iso-leucine was investigated (Fig. 1). The two structural isomers, leucine and iso-leucine, were not separated using 100 mmol L^{-1} acetic acid, but were partially separated in 850 mmol L^{-1} (5% v/v) acetic acid, and good separation was achieved using

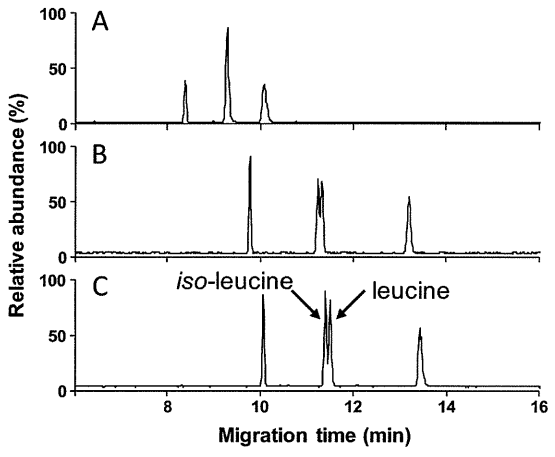

Fig. 1 Electropherograms for the separation of leucine and iso-leucine at three different BGE concentrations. (A) 100 mmol L^{-1} acetic acid; (B) 5% (v/v, 0.85 mol L^{-1}) acetic acid and (C) 10% (v/v, 1.7 mol L^{-1}) acetic acid.

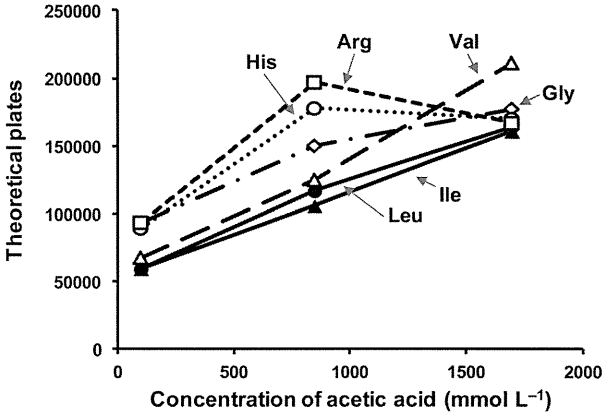

Fig. 2 Effect of acetic acid concentration on the number of theoretical plates for several amino acids.

1.7 mol L^{-1} (10% v/v) acetic acid. As reported previously,[28] at higher BGE concentrations, the number of theoretical plates for most amino acids increases (Fig. 2), so complete resolution of leucine and iso-leucine was obtained at 1.7 mol L^{-1}. The reason why the number of theoretical plates increases at higher BGE concentrations can be due to decreased interaction between the protonated analyte and capillary wall by ion exchange at lower pH. Next, the addition of methanol to the BGE was evaluated. Addition of organic solvents can reportedly reduce surface tension and provide stable spray formation,[29] and influence the signal intensity and migration times.[18] Fig. 3 depicts the changes in the signal-to-noise ratios of tryptophan, histidine and glycine with different methanol volume fractions in the BGE. The signal-to-noise ratio tended to decrease with the increase of the volume fraction of methanol, which indicates that the addition of methanol to the BGE decreases the signal intensity. These results are inconsistent with an earlier study,[18] in which the addition of methanol (volume fraction $\leq$ 30%) increased the signal intensity of hormones in a polyimide graphic coated sheathless CE-MS system. It should be noted that the analytical conditions were different from those used in the present study. In the previous report, the capillary had a relatively large i.d. (75 μm) and the BGE had a higher pH (2.85). These differences would lead to a higher BGE elution rate compared with the

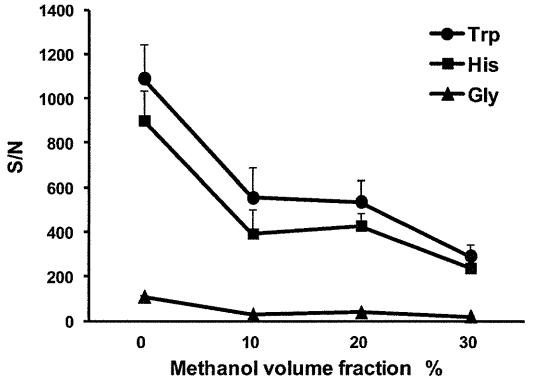

Fig. 3 Effect of addition of methanol to the BGE on the signal-to-noise ratio (*S/N*) of tryptophan (Trp), histidine (His) and glycine (Gly).

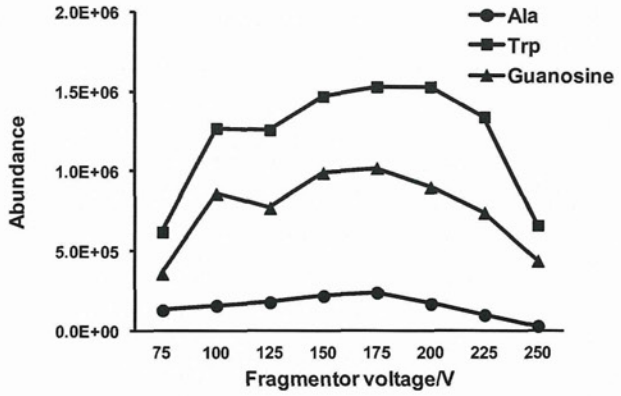

Fig. 4 Effect of the fragmentor voltage on the abundance of alanine (Ala, *m/z* 90.055), tryptophan (Trp, *m/z* 205.097) and guanosine (*m/z* 284.099).

present study, and we assume that the addition of organic solvent was necessary to stabilize the spray and obtain sufficient signal intensity in this study. Considering these observations, we selected 1.7 mol L^{-1} (10%) acetic acid without methanol as the BGE.

Optimization of the TOFMS parameters

In CE-TOFMS, the fragmentor voltage, skimmer voltage, and Oct RFV can affect sensitivity of the instrument. To optimize these parameters, a solution of three reference standards (alanine, *m/z* 90.055; tryptophan, *m/z* 205.097; guanosine, *m/z* 284.099) was infused electrokinetically by applying a CE voltage of 25 kV. Fig. 4 shows the signal intensities of the reference compounds, in which the fragmentor voltage was varied from 75 to 250 V.

At 75 V, the signal intensities of the three compounds were relatively small and there was a lot of background noise, especially at *m/z* <150. The signal intensities gradually increased as the fragmentor voltage increased, and reached their maximum values at 175 V. When the fragmentor voltage was set above 175 V, the intensities decreased, probably because of extensive fragmentation. However, in this study, we used a fragmentor

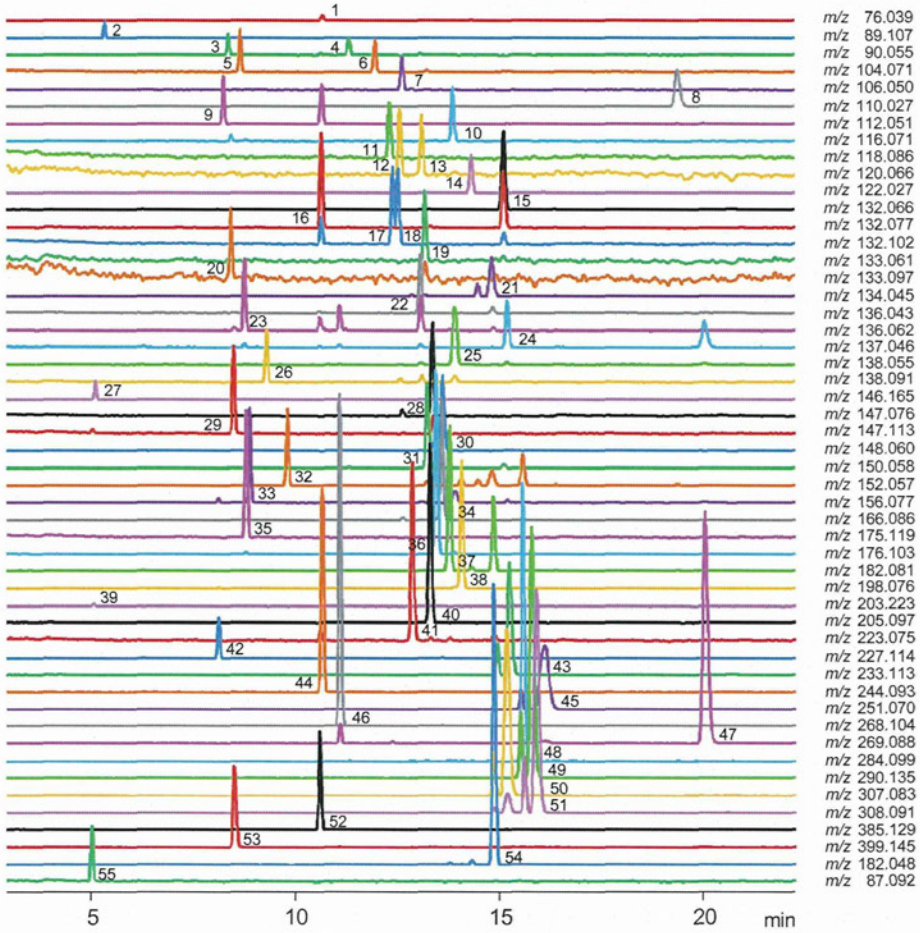

Fig. 5 Selected ion electropherograms for a standard mixture of 53 cationic metabolites obtained by sheathless CE-TOFMS. Peak identification: (1) Gly; (2) putrescine; (3) β-Ala; (4) Ala; (5) γ-aminobutyric acid; (6) 2-aminobutyric acid; (7) Ser; (8) hypotaurine; (9) cytosine; (10) Pro; (11) Val; (12) homoserine; (13) Thr; (14) Cys; (15) hydroxyproline; (16) creatine; (17) Ile; (18) Leu; (19) Asn; (20) ornithine; (21) Asp; (22) homocysteine; (23) adenine; (24) hypoxanthine; (25) anthranilate; (26) tyramine; (27) spermidine; (28) Gln; (29) Lys; (30) Glu; (31) Met; (32) guanine; (33) His; (34) Phe; (35) Arg; (36),citrulline; (37) Tyr; (38) 3,4-dihydroxyphenylalanine; (39) spermine; (40) Trp; (41) cystathionine; (42) carnosine; (43) γ-glutamyl-2-aminobutyrate; (44) cytidine; (45) γ-glutamylcysteine; (46) adenosine; (47) inosine; (48) guanosine; (49) ophthalmic acid; (50) oxidized glutathione; (51) reduced glutathione; (52) *S*-adenosylhomocysteine; (53) *S*-adenosylmethionine; (54) methionine sulfone (internal standard); (55) 3-aminopyrrolidine (internal standard). *Experimental conditions*: standard concentration, 10 μmol L^{-1} each; other experimental conditions are described in the Experimental section.

voltage of 200 V. This is because when the fragmentor voltage was set at 175 V, background noise was observed at *m/z* 82 and 105, but these interferences were considerably decreased at 200 V (data not shown). Most metabolites have molecular masses less than 300 Da, and a low background noise within this range is important for metabolome analysis.

Optimization of the skimmer voltage and Oct RFV was also investigated, but these parameters had a minimal effect on the signals of the reference compounds within the studied range. The optimized TOFMS parameters were as follows: fragmentor voltage, 200 V; skimmer voltage, 75 V; and Oct RFV, 250 V.

Method validation

Under the optimized conditions, we investigated the reproducibility, linearity and sensitivity of the sheathless CE-TOFMS method using 53 cationic metabolite standards, including amino acids and their derivatives, amines, nucleic acids and small peptides, which are predominant metabolites in biological samples. Extracted ion electropherograms of the 53 cationic metabolite standards were obtained by sheathless CE-TOFMS in positive mode using the HSPS capillary (Fig. 5). The monovalent protonated molecular $[M + H]^+$ ion peaks had the highest intensities for most of the compounds, except for oxidized glutathione, which had a higher intensity for divalent $[M + 2H]^{2+}$ than the monovalent ion.

The relative standard deviations were better than 1.4% for the migration times and between 2.4% and 18% for the normalized peak areas (Table 1). The calibration curves for all 53 cationic metabolite standards were linear with correlation coefficients between 0.9920 and 0.9999. The concentration detection limit for all species was between 0.004 and 0.8 μmol L^{-1}, which corresponds to a mass detection limit between 0.01 and 2 fmol, at a signal-to-noise ratio of three. These results indicate that the proposed method could be applied to simultaneous and quantitative analysis of cationic compounds.

Table 1 Reproducibility, linearity and sensitivity in the sheathless CE-TOFMS method

Compound	RSD (n = 10%) Migration time	Peak area	Relative peak area	Linearity correlation	Detection limit concentration (μmol L^{-1})
Gly	0.8	20	10	0.9987	0.3
Putrescine	0.7	18	14	0.9970	0.03
Ala	0.9	19	8.3	0.9987	0.2
β-Ala	0.7	18	11	0.9939	0.1
2-AB	0.9	17	6.3	0.9982	0.2
GABA	0.7	19	13	0.9992	0.1
Ser	1.0	18	6.0	0.9988	0.1
Hypotaurine	1.4	15	6.9	0.9955	0.07
Cytosine	0.7	14	6.7	0.9999	0.03
Pro	1.0	17	12	0.9993	0.08
Val	0.9	19	6.7	0.9988	0.5
Thr	0.9	18	5.4	0.9987	0.4
Homoserine	0.9	17	5.9	0.9993	0.4
Cys	1.0	19	10	0.9984	0.03
Hydroxy proline	1.1	14	6.2	0.9997	0.03
Creatine	0.8	21	10	0.9999	0.07
Ile	0.9	20	7.9	0.9994	0.2
Leu	0.9	19	9.5	0.9994	0.2
Asn	0.9	16	6.4	0.9991	0.8
Ornithine	0.7	19	16	0.9920	0.6
Asp	1.1	16	2.4	0.9957	0.09
Homocysteine	1.0	18	4.5	0.9998	0.07
Adenine	0.7	15	12	0.9994	0.04
Hypoxanthine	1.1	14	4.9	0.9993	0.2
Anthranilate	1.0	17	11	0.9965	0.03
Tyramine	0.7	14	8.5	0.9992	0.2
Spermidine	0.7	21	16	0.9944	0.03
Gln	1.0	16	4.7	0.9997	0.1
Lys	0.7	18	13	0.9997	0.09
Glu	1.0	15	4.7	0.9985	0.1
Met	1.0	18	6.2	0.9985	0.02
Guanine	0.8	13	8.4	0.9967	0.03
His	0.7	15	14	0.9986	0.03
Phe	1.0	17	6.1	0.9988	0.03
Arg	0.7	15	12	0.9998	0.06
Citrulline	1.0	14	6.1	0.9997	0.02
Tyr	1.0	13	5.3	0.9995	0.02
DOPA	1.0	13	6.6	0.9956	0.02
Spermine	0.5	22	18	0.9958	0.4
Trp	1.0	16	3.8	0.9995	0.03
Cystathionine	0.9	16	4.5	0.9992	0.07
Carnosine	0.7	17	13	0.9996	0.07
γ-Glu-2AB	1.0	14	5.3	0.9982	0.04
Cytidine	0.8	12	6.7	0.9996	0.004
γ-Glu-Cys	1.0	13	4.6	0.9961	0.05
Adenosine	0.8	11	6.0	0.9958	0.006
Inosine	1.4	12	13	0.9924	0.01
Guanosine	1.1	11	6.1	0.9982	0.004
Ophthalmate	1.1	11	6.1	0.9972	0.006
GSSG	1.1	14	4.4	0.9990	0.01
GSH	1.2	11	7.7	0.9992	0.007
SAH	0.8	19	9.4	0.9988	0.01
SAM	0.7	20	14	0.9984	0.008

Sensitivity comparison between sheath-flow and sheathless CE-TOFMS

To evaluate the sensitivity of the sheathless CE-TOFMS method, the detection limits of all species were compared among three different CE-TOFMS methods; sheath-flow CE-TOFMS with 1 mol L^{-1} formic acid, sheath-flow CE-TOFMS with 10% acetic acid, and sheathless CE-TOFMS with 10% acetic acid as BGE (Table 2). Compared with the conventional sheath-flow CE-TOFMS method with 1 mol L^{-1} formic acid, the detection limits of 21 (40%) of the compounds were at least five times better in sheathless CE-TOFMS. By contrast, the detection limits of asparagine, ornithine, tyramine and spermine decreased by half or more compared with conventional sheath-flow CE-TOFMS. Similar trends were observed between sheathless CE-TOFMS and sheath-flow CE-TOFMS methods with 10% acetic acid. The detection limits of 13 (25%) of the compounds were at least five times better in sheathless CE-TOFMS than in sheath-flow CE-TOFMS with 10% acetic acid. The detection limits of asparagine, ornithine, tyramine, spermidine and spermine were at least five times worse in the sheathless CE-TOFMS than in sheath-flow CE-TOFMS with 10% acetic acid. Decreased sensitivity in the sheathless CE-TOFMS was probably caused by high background noise. For example, the average baseline noise between 3 and 5 min in the selected ion electropherograms of asparagine in sheath-flow CE-TOFMS with 1 mol L^{-1} formic acid, sheath-flow CE-TOFMS with 10% acetic acid, and in the sheathless CE-TOFMS method was 454, 418 and 22 408, respectively. This indicates that asparagine would overlap with the high

Table 2 Sensitivity comparison among three different CE-TOFMS methods

Compound	HSPS_10% acetic acid		Sheath flow_10% acetic acid		Sheath flow_1 mol L^{-1} formic acid		Sensitivity comparison[a]	
	Detection limit concentration (μmol L^{-1})	Noise	Detection limit concentration (μmol L^{-1})	Noise	Detection limit concentration (μmol L^{-1})	Noise	HSPS *vs.* acetate	HSPS *vs.* formate
Gly	0.3	772	0.4	1604	0.7	1062	1.4	2.2
Putrescine	0.03	367	0.02	282	0.03	211	0.7	1.0
Ala	0.2	1952	0.2	818	0.4	801	0.9	1.9
β-Ala	0.1	1952	0.1	818	0.4	801	0.7	2.8
2-AB	0.2	2548	0.09	344	0.1	376	0.6	0.8
GABA	0.1	2548	0.04	344	0.1	376	0.4	1.1
Ser	0.1	2002	0.4	1287	0.8	1140	3.0	6.1
Hypotaurine	0.07	605	0.7	817	0.5	179	10.2	6.2
Cytosine	0.03	721	0.04	278	0.09	220	1.5	3.0
Pro	0.08	1815	0.2	544	0.2	532	2.1	2.9
Val	0.5	13 247	0.3	1366	0.4	1409	0.6	0.8
Thr	0.4	10 636	0.2	659	0.4	586	0.5	1.0
Homoserine	0.4	10 636	0.2	659	0.4	586	0.6	1.1
Cys	0.03	332	0.1	223	0.1	151	3.4	3.8
Hydroxyproline	0.03	785	0.1	223	0.2	241	3.7	6.2
Creatine	0.07	3429	0.05	223	0.08	208	0.7	1.1
Ile	0.2	5997	0.2	856	0.2	788	1.0	1.1
Leu	0.2	5997	0.2	856	0.2	779	0.9	1.0
Asn	0.8	22 408	0.1	418	0.3	454	0.2	0.4
Ornithine	0.6	20 033	0.1	879	0.3	864	0.2	0.4
Asp	0.09	1107	0.3	501	0.7	576	3.4	7.3
Homocysteine	0.07	1553	0.08	183	0.1	145	1.1	1.8
Adenine	0.04	1294	0.04	273	0.07	217	1.1	2.0
Hypoxanthine	0.2	2589	0.1	308	0.9	722	0.9	5.4
Anthranilate	0.03	729	0.07	218	0.09	198	2.3	2.9
Tyramine	0.2	4367	0.03	198	0.06	202	0.2	0.4
Spermidine	0.03	393	0.006	87	0.02	116	0.2	0.6
Gln	0.1	3908	0.2	464	0.3	527	1.6	3.1
Lys	0.09	3827	0.07	548	0.2	418	0.8	1.9
Glu	0.1	2549	0.2	503	0.3	525	1.7	3.3
Met	0.02	639	0.06	189	0.08	168	3.0	3.9
Guanine	0.03	929	0.05	257	0.2	326	1.6	5.7
His	0.03	1405	0.07	511	0.2	414	2.2	4.9
Phe	0.03	1283	0.1	451	0.1	406	4.3	5.1
Arg	0.06	3754	0.04	364	0.1	335	0.6	1.7
Citrulline	0.02	1131	0.06	227	0.2	222	3.7	10.3
Tyr	0.02	945	0.2	486	0.3	471	8.2	13.6
DOPA	0.02	587	0.1	242	0.1	177	4.8	5.6
Spermine	0.4	552	0.03	134	0.04	362	0.1	0.1
Trp	0.03	1583	0.1	357	0.1	232	3.4	3.8
Cystathionine	0.07	4255	0.8	2226	0.4	779	11.4	5.6
Carnosine	0.07	1706	0.09	274	0.1	400	1.2	1.3
γ-Glu-2AB	0.04	1101	0.2	340	0.2	189	6.5	4.7
Cytidine	0.004	309	0.03	169	0.08	80	7.2	18.2
γ-Glu-Cys	0.05	720	1.6	1257	1.7	1166	30.0	31.5
Adenosine	0.006	699	0.03	147	0.06	128	4.0	9.6
Inosine	0.01	596	0.2	228	0.4	195	19.6	31.7
Guanosine	0.004	285	0.05	112	0.06	78	13.8	15.5
Ophthalmate	0.006	324	0.08	177	0.1	136	14.6	18.0
GSSG	0.01	553	0.07	207	0.1	125	5.2	8.2
GSH	0.007	387	0.07	110	0.1	100	9.9	19.5
SAH	0.01	547	0.07	103	0.1	265	5.8	11.1
SAM	0.008	280	0.1	96	0.1	245	13.3	15.8

[a] Values were calculated by dividing the detection limit with both the sheath flow with 10% acetic acid and the sheath flow with 1 mol L^{-1} formic acid by that with the HSPS with 10% acetic acid.

background noise in sheathless CE-TOFMS, and this would decrease the sensitivity. The use of multiple reaction monitoring with triple quadrupole MS may improve the selectivity and reduce the high background noise.

Overall, about half of the 53 compounds tested showed increased sensitivity in the sheathless CE-TOFMS method compared with conventional methods. The sensitivity for several compounds, including γ-glutamylcysteine, inosine, guanosine, ophthalmic acid, reduced glutathione and *S*-adenosylmethionine, increased more than 10 times compared with both the sheath-flow methods. The *m/z* values of these compounds were above 250 where no significant background noise was observed, and this facilitated the increase in sensitivity in the sheathless method.

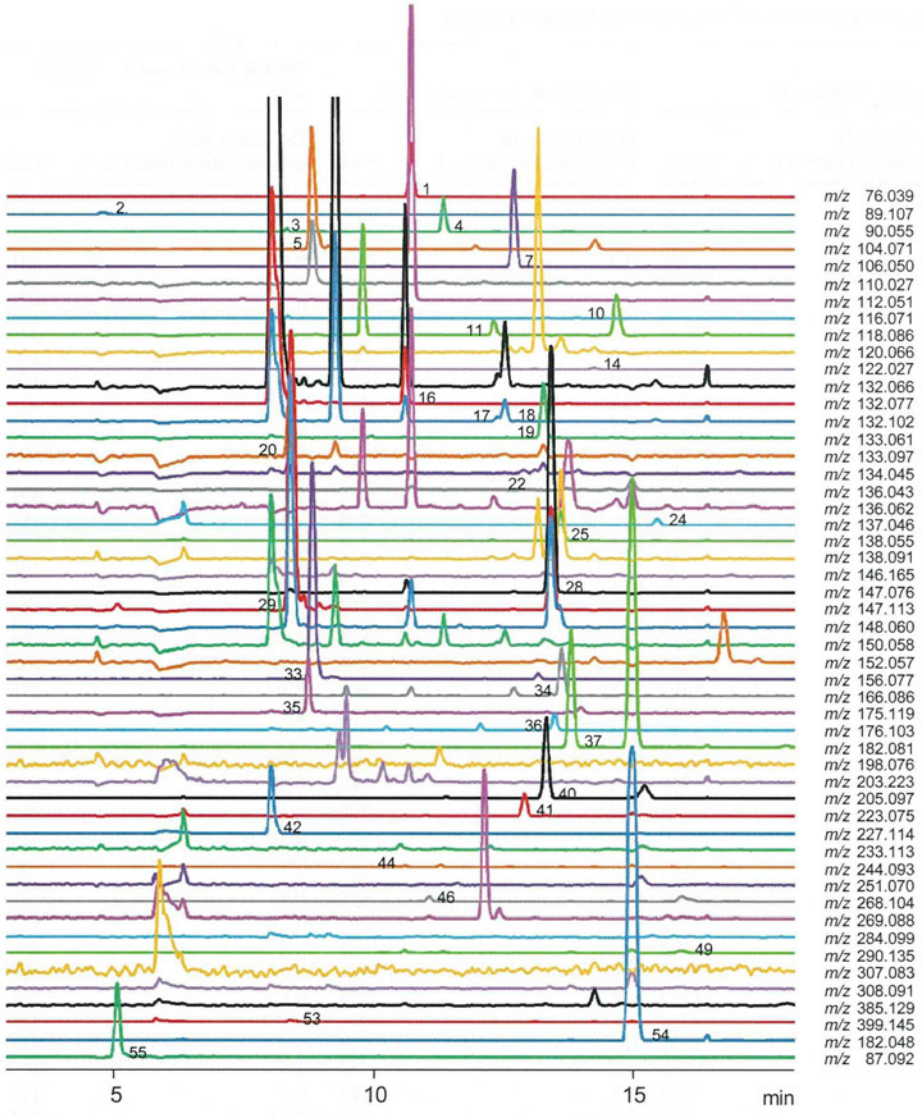

Fig. 6 Selected ion electropherograms of cationic metabolites in human urine. Peak identifications are the same as in Fig. 5. Experimental conditions are described in the Experimental section.

Application to metabolome analysis of human urine

The sheathless CE-TOFMS method was applied to metabolome analysis of human urine. Fig. 6 shows the selected ion electropherograms of 53 cationic compounds in human urine from a healthy volunteer that was analyzed by sheathless CE-TOFMS. The 31 compounds were identified by matching their molecular masses and migration times with those of standards. The number of peaks detected with sheath-flow CE-TOFMS with 1 mol L^{-1} formic acid and sheathless CE-TOFMS were compared. Setting a threshold value of a signal-to-noise of three, 1659 peaks were detected with the sheath-flow CE-TOFMS method, while 16 147 peaks were detected with sheathless CE-TOFMS on average (Table 3). The number of peaks detected in all signal-to-noise ratio categories for the sheathless method was more than seven times compared with the sheath-flow method. This indicates that the sheathless method is more effective than the sheath-flow method for the detection of small peaks. Finally, the robustness of the HSPS capillary was investigated. For over 180 successive analyses only a slight drop in the current and small fluctuations in the migration time were observed, and the capillary did not require any modifications except for changing the BGE. Overall, sheathless CE-MS provides a several-fold increase in sensitivity for compounds with *m/z* >250. If elimination of background noise in the region below *m/z* 250 is possible, this method could be a powerful tool for metabolome analysis.

Experimental

Chemicals

Methionine sulfone (internal standard) was purchased from Alfa Aesar (Ward Hill, MA), ophthalmate from Bachem (Bubendorf, Switzerland), hexakis-(2,2-difluorothoxy)-phosphazene (hexakis) from SynQuest Laboratories (Alachua, FL), and 2-aminobutyrate, hypotaurine, cytosine, homocysteine, hypoxanthine, cystathionine, *S*-adenosylhomocysteine and 3-aminopyrrolidine (reference compound) from Sigma-Aldrich (St Louis, MO).

Table 3 Number of peaks detected from human urine with sheathless and sheath-flow methods

	Sheath-flow				Sheathless			
	Sample A	Sample B	Sample C	Average	Sample A	Sample B	Sample C	Average
Total	2039	1328	1609	1659	18 796	16 268	13 378	16 147
$3 < S/N \leqq 10$	1231	826	962	1006	12 606	12 395	9624	11 542
$10 < S/N \leqq 100$	732	449	594	592	5547	3510	3408	4155
$100 < S/N$	76	53	53	61	643	363	346	451

γ-Glutamylcysteine and γ-glutamyl-2-aminobutyrate were synthesized at the Toray Research Center (Tokyo, Japan). All other reagents were obtained from Wako Pure Chemicals Industries Ltd. (Osaka, Japan). All chemicals used were of analytical or reagent grade. Stock solutions (1–100 mmol L^{-1}) were prepared in either Milli-Q (Millipore, Billerica, MA) water, aqueous 0.1 mol L^{-1} HCl, or aqueous 0.1 mol L^{-1} NaOH. The working mixture standard was prepared by diluting these stock solutions with Milli-Q water just before analysis.

Sample preparation

Urine samples were collected from a healthy volunteer. An aliquot (20 μL) of the urine sample was placed in a tube and mixed with 20 μL of an aqueous solution of methionine sulfone (2 mmol L^{-1}) and 3-aminopyrrolidine (2 mmol L^{-1}), and 160 μL of Milli-Q water. The solution was then centrifugally filtered through a 5 kDa cutoff filter (Millipore) to remove proteins. The filtrate was used for subsequent CE- time-of-flight mass spectrometry (TOFMS).

Instrumentation

The sheathless CE-TOFMS experiments were carried out with a PA 800 *plus* capillary electrophoresis system (Beckman Coulter) and an Agilent 6220 Accurate-Mass TOF LC/MS system (Agilent Technologies, Palo Alto, CA).

The sheath-flow CE-TOFMS experiments were performed using an Agilent CE capillary electrophoresis system equipped with an Agilent 6220 Accurate-Mass TOF LC/MS system, an Agilent 1100 series isocratic HPLC pump, an Agilent CE-MS adapter kit, and an Agilent CE-ESI-MS sprayer kit (Agilent Technologies).

Sheathless CE-TOFMS conditions

A prototype HSPS (fused-silica, 30 μm i.d., 150 μm o.d., 90 cm total length) with a porous segment (approximately 3 cm) on its outlet terminal was supplied by Beckman Coulter (Fig. 7). The HSPS capillary was inserted into a stainless steel ESI needle to enable electrical contact between the electrolyte and conductive liquid *via* a secondary capillary (fused-silica, 50 μm i.d., 360 μm o.d., 80 cm total length). A nanospray end cap and a gas diverter were installed instead of the standard ESI end cap.

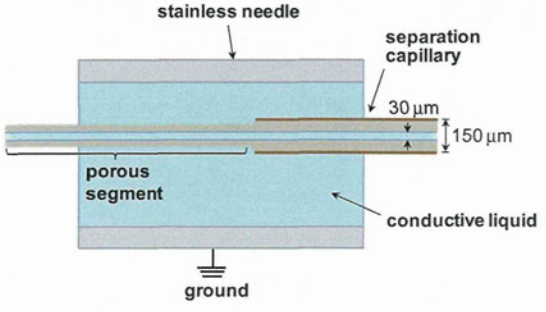

Fig. 7 Schematic representation for the high-sensitivity porous sprayer interface.

Before use, the new capillary was successively flushed at 345 kPa with methanol (5 min), Milli-Q water (5 min), 0.1 mol L^{-1} hydrochloric acid (5 min), Milli-Q water (5 min), 1 mol L^{-1} sodium hydroxide (30 min), Milli-Q water (5 min) and BGE (5 min). The HSPS was then placed on a *xyz* stage, and the position of the tip was optimized by maximizing the signals for three reference compounds (leucine, tryptophan and guanosine) under continuous electrophoresis.

Aqueous acetic acid (10% v/v, pH 2.2) was used as the BGE and conductive liquid. Between runs, the capillary was flushed with the BGE for 5 min at 345 kPa, and then the stainless steel ESI needle was refilled with conductive liquid for 0.5 min at 345 kPa. The sample solution (2.6 nL) was injected at 20.7 kPa for 5 s. A constant separation voltage of 25 kV was applied after it was increased from 0 to 25 kV over the first minute of the analysis. The capillary was maintained at room temperature (25 °C), and the sample tray was cooled to 10 °C.

ESI-TOFMS was conducted in positive ion mode and the capillary voltage was set at a value between 850 and 950 V, which depended on the distance between the porous tip and the MS inlet. For TOFMS, the optimized fragmentor voltage, skimmer voltage, and octupole radio frequency voltage (Oct RFV) were 200 V, 75 V, and 250 V, respectively. An automatic recalibration function was performed using the following two reference masses: an ammonium adduct ion of acetic acid, $(CH_3COOH + NH_4)^+$, *m/z* 78.05493; and protonated di-sec-octyl phthalate, $(C_{24}H_{38}O_4 + H)^+$, *m/z* 391.28429. Exact mass data were acquired at a rate of 1.5 spectra per second from *m/z* 50 to 1000.

Sheath-flow CE-TOFMS conditions

Conventional sheath-flow CE-MS was carried out as previously described.[9,28] Briefly, samples were separated in a fused-silica capillary (50 μm i.d., 360 μm o.d., 100 cm total length) filled with either 1 mol L^{-1} formic acid or 10% (v/v) aqueous acetic acid (pH 2.2) as the BGE. The sample solution was injected at 5 kPa for 3 s (2.3 nL) and a positive voltage of 30 kV was applied. The temperatures of the capillary and the sample tray were maintained at 20 °C and 5 °C, respectively. The sheath liquid was methanol–water (50% v/v) containing 0.1 μmol L^{-1} hexakis with a flow rate of 10 μL min^{-1}.

ESI-TOFMS was operated in positive ion mode and the capillary voltage was set at 4 kV. A capillary gas (dry nitrogen)

heated to 300 °C was used at a flow rate of 7 L min^{-1}. In TOFMS, the fragmentor voltage, skimmer voltage and Oct RFV were set at 75, 50 and 125 V, respectively. Automatic recalibration of each acquired spectrum was performed using the masses of the following reference standards: ^{13}C isotopic ion of protonated methanol dimer, $(2CH_3OH + H)^+$, *m/z* 66.06306; and $(hexakis + H)^+$, *m/z* 622.02896. Exact mass data were acquired at 1.5 spectra per second from *m/z* 50 to 1000.

Data analysis

The acquired raw CE-TOFMS data were analyzed using our proprietary software for quantitation of metabolites.[11] Peak identification was performed by matching the *m/z* values and normalized migration times with those of standard reagents.

Conclusions

A sheathless CE-MS with a HSPS capillary was evaluated for the analysis of cationic metabolites. Satisfactory resolution was achieved for validation of compounds using 10% aqueous acetic acid as the BGE. The method had good reproducibility, linearity and sensitivity, which allowed detection of cationic metabolites at levels of several femtomoles or lower. Compared with conventional sheath-flow CE-MS, although a decrease in sensitivity was observed for some metabolites, the sheathless approach increased the sensitivity by more than 5-fold for 40% of the metabolites analyzed. The method was applied to the analysis of cationic metabolites in human urine. The number of peaks detected was 10 times that with conventional methods, and more than 180 successive runs were conducted without any problems. These results indicate that the proposed sheathless CE-MS method is promising for metabolome analysis of cationic species in many areas.

Acknowledgements

We thank John C. Hudson, Lena Sripitisawad, Jean-Marc Busnel, Jerald S. Feitelson, and Etsuo Arai (Beckman Coulter, Inc) for providing the HSPS sprayer interface and technical support. We also thank Dr Cheng Kian Kai (Institute for Advanced Biosciences, Keio University) for critical reading of the manuscript. This work was supported financially by the Yamagata Prefectural Government and the City of Tsuruoka.

References

1 H. L. Chuang, Y. T. Huang, C. C. Chiu, C. D. Liao, F. L. Hsu, C. C. Huang and C. C. Hou, *J. Nutr. Biochem.*, 2012, **23**, 752–758.
2 M. Ooi, S. Nishiumi, T. Yoshie, Y. Shiomi, M. Kohashi, K. Fukunaga, S. Nakamura, T. Matsumoto, N. Hatano and M. Shinohara, *Inflammation Res.*, 2011, 1–10.
3 S. U. Bajad, W. Lu, E. H. Kimball, J. Yuan, C. Peterson and J. D. Rabinowitz, *J. Chromatogr., A*, 2006, **1125**, 76–88.
4 P. Bernini, I. Bertini, C. Luchinat, L. Tenori and A. Tognaccini, *J. Proteome Res.*, 2011, **10**, 4983–4992.
5 W. C. Yang, F. E. Regnier and J. Adamec, *Electrophoresis*, 2008, **29**, 4549–4560.
6 T. Soga, Y. Ueno, H. Naraoka, Y. Ohashi, M. Tomita and T. Nishioka, *Anal. Chem.*, 2002, **74**, 2233–2239.
7 T. Soga, Y. Ohashi, Y. Ueno, H. Naraoka, M. Tomita and T. Nishioka, *J. Proteome Res.*, 2003, **2**, 488–494.
8 T. Soga, R. Baran, M. Suematsu, Y. Ueno, S. Ikeda, T. Sakurakawa, Y. Kakazu, T. Ishikawa, M. Robert, T. Nishioka and M. Tomita, *J. Biol. Chem.*, 2006, **281**, 16768–16776.
9 A. Hirayama, K. Kami, M. Sugimoto, M. Sugawara, N. Toki, H. Onozuka, T. Kinoshita, N. Saito, A. Ochiai, M. Tomita, H. Esumi and T. Soga, *Cancer Res.*, 2009, **69**, 4918–4925.
10 T. Soga, K. Igarashi, C. Ito, K. Mizobuchi, H. P. Zimmermann and M. Tomita, *Anal. Chem.*, 2009, **81**, 6165–6174.
11 M. Sugimoto, D. T. Wong, A. Hirayama, T. Soga and M. Tomita, *Metabolomics*, 2010, **6**, 78–95.
12 T. Soga, M. Sugimoto, M. Honma, M. Mori, K. Igarashi, K. Kashikura, S. Ikeda, A. Hirayama, T. Yamamoto, H. Yoshida, M. Otsuka, S. Tsuji, Y. Yatomi, T. Sakuragawa, H. Watanabe, K. Nihei, T. Saito, S. Kawata, H. Suzuki, M. Tomita and M. Suematsu, *J. Hepatol.*, 2011, **55**, 896–905.
13 M. Moini, *Anal. Bioanal. Chem.*, 2002, **373**, 466–480.
14 Z. Kele, G. Ferenc, E. Klement, G. K. Toth and T. Janaky, *Rapid Commun. Mass Spectrom.*, 2005, **19**, 881–885.
15 M. S. Kriger, K. D. Cook and R. S. Ramsey, *Anal. Chem.*, 1995, **67**, 385–389.
16 Y. R. Chen and G. R. Her, *Rapid Commun. Mass Spectrom.*, 2003, **17**, 437–441.
17 A. D. Zamfir, N. Dinca, E. Sisu and J. Peter-Katalinic, *J. Sep. Sci.*, 2006, **29**, 414–422.
18 V. Sanz-Nebot, E. Balaguer, F. Benavente and J. Barbosa, *Electrophoresis*, 2005, **26**, 1457–1465.
19 P. Cao and M. Moini, *J. Am. Soc. Mass Spectrom.*, 1997, **8**, 561–564.
20 Z. Chen, B. Boggess and H. C. Chang, *J. Mass Spectrom.*, 2007, **42**, 244–253.
21 L. H. Shi, Y. X. Jin, D. C. Moon, S. K. Kim and S. R. Park, *Electrophoresis*, 2009, **30**, 1661–1669.
22 M. Moini, *Anal. Chem.*, 2007, **79**, 4241–4246.
23 J. M. Busnel, B. Schoenmaker, R. Ramautar, A. Carrasco-Pancorbo, C. Ratnayake, J. S. Feitelson, J. D. Chapman, A. M. Deelder and O. A. Mayboroda, *Anal. Chem.*, 2010, **82**, 9476–9483.
24 K. Faserl, B. Sarg, L. Kremser and H. Lindner, *Anal. Chem.*, 2011, **83**, 7297–7305.
25 R. Haselberg, C. K. Ratnayake, G. J. de Jong and G. W. Somsen, *J. Chromatogr., A*, 2010, **1217**, 7605–7611.
26 M. Kawai, Y. Iwamuro, R. Iio-Ishimaru, S. Chinaka, N. Takayama and K. Hayakawa, *Anal. Sci.*, 2011, **27**, 857–860.
27 R. Ramautar, J. M. Busnel, A. M. Deelder and O. A. Mayboroda, *Anal. Chem.*, 2012, **84**, 885–892.
28 T. Soga and D. N. Heiger, *Anal. Chem.*, 2000, **72**, 1236–1241.
29 J. Samskog, M. Wetterhall, S. Jacobsson and K. Markides, *J. Mass Spectrom.*, 2000, **35**, 919–924.

International Journal of Cardiology 161 (2012) 130–136

Contents lists available at ScienceDirect

International Journal of Cardiology

journal homepage: www.elsevier.com/locate/ijcard

Analysis of liver metabolism in a rat model of heart failure ☆

Takao Kato [a,b], Shinichiro Niizuma [a], Yasutaka Inuzuka [a], Tsuneaki Kawashima [a], Junji Okuda [a], Akira Kawamoto [a], Yodo Tamaki [a], Yoshitaka Iwanaga [a], Tomoyoshi Soga [c], Toru Kita [a], Takeshi Kimura [a], Tetsuo Shioi [a,*]

[a] Department of Cardiovascular Medicine, Graduate School of Medicine, Kyoto University, Kyoto, Japan
[b] Division of Cardiology, The Tazuke Kofukai Medical Reseach Institute, Kitano Hospital, Osaka, Japan
[c] Institute for Advanced Bioscience, Keio University, Yamagata, Japan

ARTICLE INFO

Article history:
Received 28 December 2010
Received in revised form 5 July 2011
Accepted 10 July 2011
Available online 11 August 2011

Keywords:
Heart failure
Cachexia
Liver
Lipogenesis
Inflammation

ABSTRACT

Background: Cachexia, namely body wasting, is a common complication in cases of congestive heart failure (CHF). Although, neurohumoral and immune abnormalities are associated with the condition, precisely how the imbalance of catabolism and anabolism is responsible for the wasting process is not known.
Methods: We analyzed markers of cachexia in Dahl salt-sensitive rats which show marked hypertension with preserved systolic function at 11 weeks and CHF at 17–19 weeks of age. We also analyzed the change in hepatic metabolism associated with CHF since liver plays a central role in the systemic regulation of catabolism and anabolism.
Results: In CHF rats, a failure to grow was observed and blood hepatic protein levels were decreased associated with increased blood proinflammatory cytokine levels, indicating that Dahl rats serve as a model of cardiac cachexia. Food intake was reduced, and blood sugar and insulin levels were decreased. Despite the apparent fasting condition, blood fatty acid levels were decreased and triglycerides levels were increased. In CHF rats, liver incorporated more glucose, the gene expression related to gluconeogenesis was decreased, the gene expression related to lipogenesis was increased, and the triglyceride content of the liver was increased. The paradoxical production of triglycerides synthesis in fasting rats was associated with a proinflammatory response in liver.
Conclusions: The Dahl salt-sensitive rat can be used as a model of cardiac cachexia. The cachexia was associated with abnormal hepatic metabolism that might work as a maladaptive response during the progression of CHF.

1. Introduction

Congestive heart failure (CHF) is becoming a serious health care problem. CHF is associated with a significant change in energy metabolism of the heart, and the altered energetics is hypothesized to play an important role in the progression of CHF [1]. Using a Dahl rat model which shows a distinct transition from compensated left ventricular hypertrophy to CHF, we recently found that left ventricular hypertrophy or CHF was associated with a distinct change in the metabolic profile of the heart and that the metabolic remodeling of heart might be a therapeutic target [2].

CHF is also associated with abnormal energy metabolism in extra-cardiac tissues. Cachexia, namely body wasting, is a common complication among CHF patients [3,4]. Cardiac cachexia is associated with a poor prognosis and disability. Several lines of evidence suggest that neurohumoral and immune abnormalities play a critical role, and a complex imbalance of catabolism and anabolism is likely to be responsible for the development of the wasting process [4].

Although cardiac cachexia is an important complication and a potential target of therapeutic intervention in cases of CHF, its pathophysiology is poorly understood. One reason for this is the limited number of animal models of cardiac cachexia available. There is a report that the skeletal muscle atrophy caused by reduced activity is significantly different from the muscle atrophy observed in CHF rats [5]. However, the mechanism by which the imbalance between catabolism and anabolism is induced is not clear. In this study, we have shown that the Dahl salt-sensitive rat fed a high-salt diet is an animal model of cardiac cachexia. To gain insight into the mechanism of cardiac cachexia, we have analyzed the change of hepatic

☆ Grant support: Grants from the Japan Society for the Promotion of Science, Japan Heart Foundation, Japan Foundation of Cardiovascular Research, NOVARTIS Foundation for the Promotion of Science, Mochida Memorial Foundation for Medical and Pharmaceutical Research, Takeda Science Foundation, and Vehicle Racing Commemorative Foundation.

* Corresponding author at: Department of Cardiovascular Medicine, Graduate School of Medicine, Kyoto University, 54 Shogoinkawahara-cho, Sakyo-ku, Kyoto 606-8507, Japan. Tel.: +81 75 751 3670; fax: +81 75 751 3203.
E-mail address: tshioi@kuhp.kyoto-u.ac.jp (T. Shioi).

0167-5273/$ – see front matter © 2011 Elsevier Ireland Ltd. All rights reserved.
doi:10.1016/j.ijcard.2011.07.056

Table 1
Primer sequences used in real time quantitative RT-PCR.

Gene	Forward	Reverse	Ref.	GenBank entry
18SrRNA	AGTCCCTGCCCTTTGTACACA	CGATCCGAGGGCCTCACTA	[26]	M11188
Pyruvate carboxylase	CCGTTCTAAGGTGCTAAAGGA	GACGAGTATTCAGGCTATCCA		BC085680.1
Phosphoenolpyruvate carboxykinase (PEPCK)	ATGTCAGAAGAGGACTTCGAGA	CTCAATACCAATCTTGGCCAGA		BC085680.1
ATP Citrate lyase	GGCAAGATCCTCATCATTGGA	CAACTTCTCCCATCACTCGTA		BC100618.1
Acetyl-CoA carboxylase (ACC) α	ATGATTGCTGGGGAATCCTCA	GAGGTGTATACTTCCCGACCA		NM_022193.1
Fatty acid synthase	CAAGTTATTCGACCACCCAGA	TCACCCAGTTGTCTTTCCAGA		NM_017332.1
Sterol regulatory element-binding protein (SREBP) 1c	TCACTGAAAGACCTGGTGTCA	GCTTTCACCTGGTTATCCTCA		AF286470.2
Sterol regulatory element-binding protein (SREBP) 2	CAAGTACCTGCAGCAGGTCA	AGTCAATGGAATAGGGGGAGA		NM_001033694
Tumor necrosis factor (TNF)α	ATGGTCCTCTTTCAGTCG GAG	TGTC TACTGAACTTCGGGGTG	[27]	NM_012675.3
Interleukin (IL)1β	CTTCCCCAGGACATGCTAGG	CAAAGGCTTCCCCTGGAGAC	[28]	NM_031512.2
C-reactive protein (CRP)	ACATTGTGGGGACAAATGCA	ACATTGGGGCTGAATACCCTA		NM_017096.3
Transthyretin	GGCTCACCACAGATGAGAAGTTC	ACAAATGGGAGCTACTGCTTTGGC	[29]	NM_012681.1
Retinol-binding protein (RBP) 4	AGAAGGGTCATATGAGCGCTA	GTATCGATGATCCAGTGGTCA		NM_013162.1
Hepatocyte nuclear factor (HNF) 4	AAATGTGCAGGTGTTGACCA	CACGCTCCTCCTGAAGAATC	[29]	EF193392

metabolism since the liver plays a central role in the systemic regulation of catabolism and anabolism.

2. Materials and methods

2.1. Animals

Inbred male Dahl salt-sensitive (DS) rats (Japan SLC, Hamamatsu, Shizuoka, Japan) were fed a 0.3% NaCl (low salt; LS) diet until the age of 6 weeks, then an 8% NaCl (high salt; HS) diet [2]. DS rats fed only the low-salt diet were used as controls. Animal care and the experiments were approved by the Institutional Animal Care and Use Committee of Kyoto University and conducted by the Guide for the Care and Use of Laboratory Animals published by the United States National Institutes of Health.

2.2. Protocols

Serial measurements of body weight, food intake, and cardiac function by echocardiography were performed from 11 weeks of age. Blood samples were obtained at age 18 weeks without fasting. The measurement of mRNAs, proteins, and metabolites was performed at the age of 11 and 18 weeks without fasting. The hepatic uptake of ^{18}F-deoxyglucose (FDG) and ^{125}I-15-(*p*-iodophenyl)-9-*R,S*-methylpentadecanoic acid (9MPA) was measured at age 11 and 18 weeks after an overnight fast.

2.3. Cardiac echocardiography

Echocardiography was performed based on a previously reported protocol [2]. Briefly, rats were anesthetized with inhaled diethyl ether (Wako Pure Chemical Industries, Osaka, Japan), and transthoracic echocardiography was performed using a Sonos-5500 echocardiograph (Agilent Technologies, Santa Clara, CA) with a 15-MHz linear transducer. M-mode echocardiograms were obtained at the papillary muscle level. At least two independent M-mode measurements for each animal were carried out.

2.4. Blood analysis

Blood samples were collected without fasting via the right ventricle, and the samples were centrifuged at 3000 rpm for 15 min and analyzed as described [2]. Plasma concentration of insulin was analyzed using a commercial kit (Shibayagi Co., Shibukawa, Gunma, Japan).

2.5. Sampling of hepatic tissue

To obtain liver tissues for biochemical analyses, 11-week-old LS (n = 6), 11-week-old HS (n = 8), and 17-week-old HS (n = 6) rats were sacrificed by decapitation without fasting. A piece of the liver was obtained from the right lobe, rapidly divided, snap frozen in liquid nitrogen, and stored at −80 °C. The liver tissues were also used for the measurement of mRNA, glycogen, and triglyceride (TG).

2.6. Metabolome analysis (CE-TOFMS)

A targeted metabolomic approach was performed using capillary electrophoresis time-of-flight mass spectrometry (CE-TOFMS) [6]. Hepatic tissue from 11-week-old LS (n = 6), 11-week-old HS (n = 6), and 17-week-old HS (n = 6) rats were analyzed. The conditions used were described in Supplementary materials.

2.7. Levels of glycogen and triglycerides

Glycogen and TGs were extracted from liver tissue of 11-week-old LS, 11-week-old HS, and 17-week-old HS rats (n = 6–8 in each group) using previously described methods [7,8], and analyzed with commercial kits (BioAssay Systems, Hayward, CA, and Cayman Chemical, Ann Arbor, MI, respectively).

2.8. Quantitative reverse transcription-polymerase chain reaction (RT-PCR)

Total RNA was isolated from the liver tissue (n = 6–8 in each group) by the acid guanidinium thiocyanate–phenol–chloroform method. Quantitative RT-PCR was carried out as described previously [2]. The sequences of primers used are listed in Table 1. The mRNA level of each gene was standardized with the corresponding 18S ribosomal RNA as an internal control. The Genbank accession numbers are also included in Table 1.

2.9. Western blotting

Liver lysate was obtained by homogenization in ice-cold buffer [10% glycerol, 137 mM NaCl, 20 mM Tris–HCl pH 7.4, 4 g/ml aprotinin, 4 g/ml leupeptin, 1 mM phenylmethylsulfonyl fluoride (PMSF), 4 g/ml pepstatin, 20 mM NaF, 1 mM sodium pyrophosphate, and 1 mM orthovanadate] [9]. The lysate was kept on ice for 15 min and cleared by centrifugation at 15,000 g for 20 min at 4 °C. Protein concentrations were determined by the Bradford method (BioRad, Hercules, CA). 200 μg of liver tissue lysate was subjected to sodium dodecyl sulfate-polyacrylamide gel electrophoresis (SDS-PAGE), and the proteins were transferred onto polyvinylidene difluoride membranes. The primary antibodies used for western blotting were for sterol regulatory element-binding protein (SREBP) 1 (2A4, 1:500, Santa Cruz, Santa Cruz, CA), SREBP2

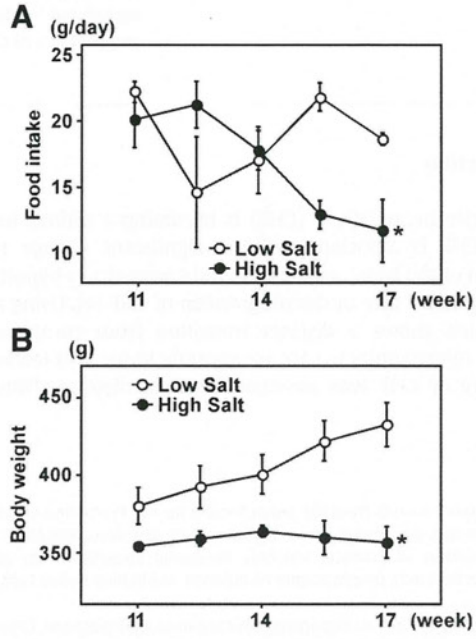

Fig. 1. Food intake and body weight of Dahl rats fed a high-salt diet. (A) Serial measurements of food intake. Rats with congestive heart failure (CHF) ate less than control rats. (B) Serial measurements of body weight. CHF rats showed a failure to grow. n = 4 for each group. *p < 0.05 versus control rats, namely Dahl rats fed a low-salt diet.

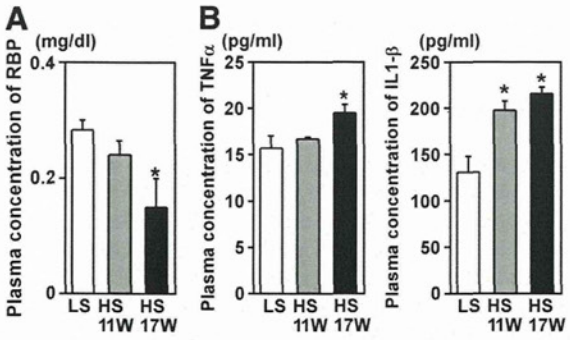

Fig. 2. Markers of cachexia in Dahl rats. (A) The concentration of retinol-binding protein (RBP) in plasma was decreased in CHF rats (HS 17W). (B) The plasma concentration of tumor necrosis factor (TNF)-α and interleukin (IL)1-β was increased in CHF rats. n = 6–8 in each group. LS; low salt, HS; high salt. *p<0.05 versus control LS rats.

(1:500, (Cayman Chemical), and glyceraldehyde-3-phosphate dehydrogenase (GAPDH; 1:1000, Chemicon, Temecula, CA).

2.10. Hepatic uptake of ^{18}FDG and ^{125}I-9MPA

The hepatic uptake of glucose and fatty acids was estimated by measuring the incorporation of an analog of glucose (deoxyglucose) and a fatty acid (9MPA) as described [2]. The 11-week-old LS (n = 7), 11-week-old HS (n = 10), and 17-week-old HS rats (n = 12) were injected with 1 mCi of ^{18}FDG and 20 μCi of ^{125}I-9MPA. The animals were fasted overnight before the injection since variation in the uptake of the isotope-labeled molecule was found when fed animals were used. The rats were sacrificed by decapitation 45 min after the injection, and the livers were removed and washed in cold saline. Specimens of the left lobe were collected and frozen in liquid nitrogen and radioisotopic activity was measured using a scintillation counter (Packard Cobra2 ™ Auto-gamma, GMI, Ramsey, Minnesota) [2]. To measure ^{18}FDG uptake, radioisotopic activity was measured just after sacrifice because the half decay time of ^{18}FDG is 110 min. To measure ^{125}I-9MPA uptake, another radioisotopic measurement was made 48 h after the first. The amount of radioisotope incorporated was presented as a percentage of the administered dose corrected by liver weight in grams. Using this method, cross-talk between the two tracers was negligible [2].

2.11. Plasma and tissue concentrations of inflammatory cytokines

The levels of tumor necrosis factor (TNF)-α and interleukin (IL)1-β in tissue homogenate and plasma were measured using sandwich enzyme-linked immunosorbent assay (ELISA) kits (Shibayagi Co. and R&D Systems; Minneapolis, MN), according to the manufacturers' instructions. The tissue homogenate for the protein analysis was used in this assay.

2.12. Statistical analysis

Values are expressed as means ± SEMs. Differences among experimental groups were tested by ANOVA with post hoc comparisons using the Bonferroni test. In all tests, a value of $p<0.05$ was considered significant.

3. Results

3.1. Dahl rats fed a high-salt diet develop hypertension, heart failure, and cachexia

As we reported previously, DS rats fed a high-salt (HS) diet developed hypertension (HT) at 11 weeks of age (systolic blood pressure; 211 ± 12 mm Hg, diastolic blood pressure; 160 ± 6 mm Hg) [2]. On echocardiographic examination, fractional shortening (FS) was

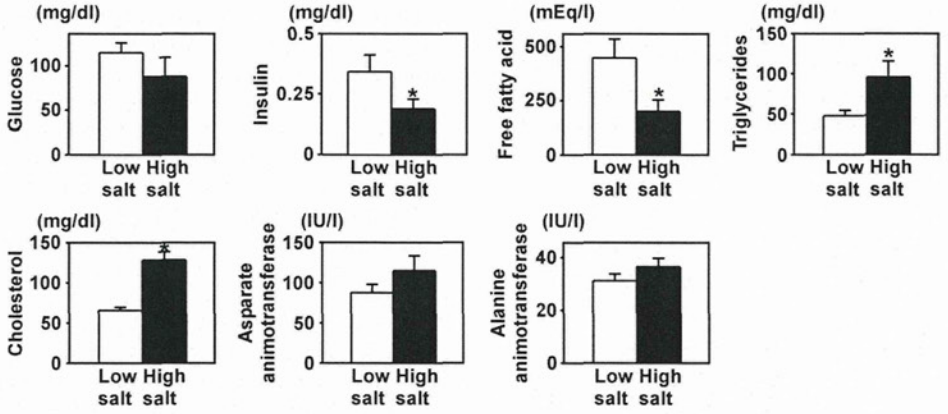

Fig. 3. Blood analysis of Dahl rats. Blood sugar and insulin levels were decreased, and triglyceride and cholesterol levels were increased in CHF rats. n = 5–6 in each group. *p<0.05 versus control rats.

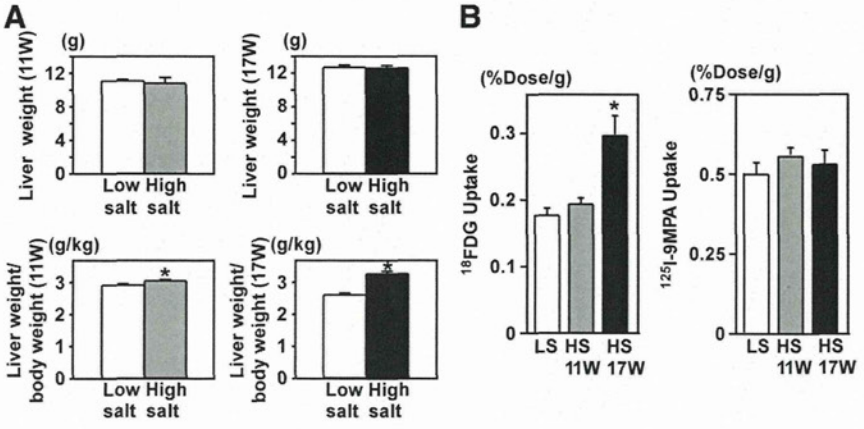

Fig. 4. Liver weight and the uptake of glucose and fatty acids. (A) Liver weight and liver weight corrected by body weight at 11 and 17 weeks of age. Liver weight corrected by body weight was increased in CHF rats (HS 17W) compared with control rats. n = 6–12 in each group. LS; low salt, HS; high salt. *p<0.05 versus control rats. (B) The uptake of ^{18}FDG, a glucose analog, was increased in CHF rats (HS 17W) compared to control rats. The uptake of ^{125}I-9MPA, a fatty acid analog, in the liver was not changed. n = 7–12 in each group. *p<0.05 versus control rats.

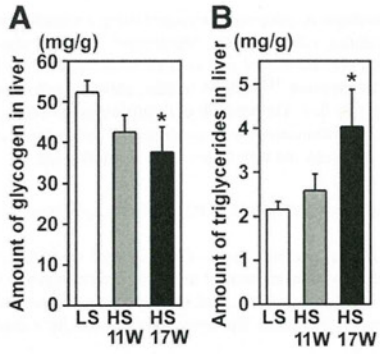

Fig. 5. Glycogen and triglyceride content in liver. (A) The amount of glycogen in liver was decreased in CHF rats. (B) The amount of triglycerides in liver was increased in CHF rats. n = 6–8 in each group. LS; low salt, HS; high salt. *p<0.05 versus control rats.

found to be preserved (62.4 ± 0.9%). At around 17 weeks of age, the rats showed signs of CHF, such as tachypnea and immobilization, and decreased FS (39.7 ± 1.5%). DS rats fed a low-salt (LS) diet did not develop hypertension or CHF, and were used as controls.

Serial measurements of food intake and body weight showed that CHF rats ate less than controls (Fig. 1A) and had a lower body weight (Fig. 1B). The failure to grow in the CHF rats led us hypothesize that the animals may serve as a model of cardiac cachexia. Blood levels of hepatic proteins, such as albumin, transthyretin, and transferrin, can serve as markers of a nutritional index to screen for malnutrition and monitor the metabolic response to dietary intervention [10,11]. Blood hepatic proteins are synthesized mainly in liver and have short half lives in blood. We measured the concentration of retinol-binding protein (RBP), a blood hepatic protein, in plasma and found that it was decreased in CHF rats (Fig. 2A). Cachexia is also known to be associated with neurohumoral and immune abnormalities [4]. Indeed, plasma concentrations of two representative proinflammatory cytokines, TNF-α and IL-1β, were elevated in CHF rats (Fig. 2B).

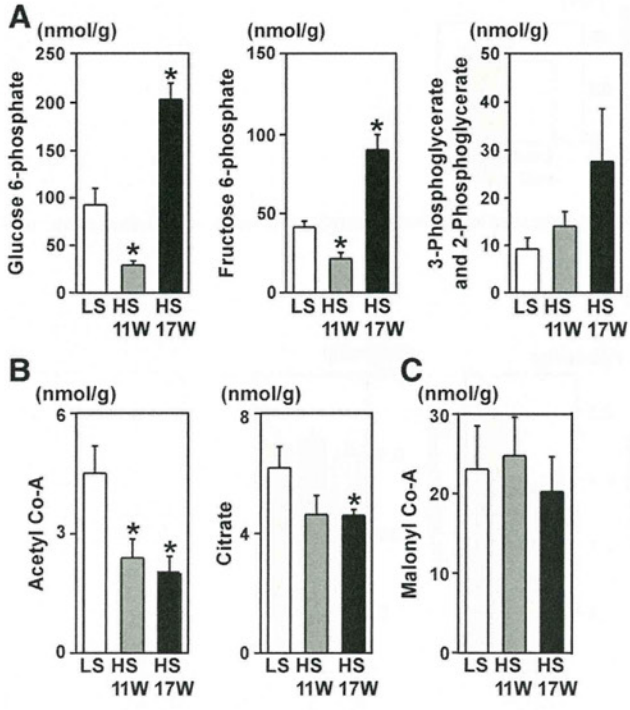

Fig. 6. The amounts of metabolites in liver determined by metabolome analysis. (A) Concentrations of metabolites of glycolysis. (B) Concentrations of metabolites in the Krebs cycle. (C) Malonyl CoA concentration. n = 6 in each group. LS; low salt, HS; high salt. *p<0.05 versus control rats.

3.2. Blood analysis of CHF rats

To investigate the systemic metabolic profile of Dahl rats, we examined blood chemistry. Both glucose and insulin levels were lower in CHF rats than control rats in the fed condition (Fig. 3), as reported [2]. Plasma levels of cholesterol and TG were increased, and free fatty acids (FFAs) were decreased in DS rats with CHF, as reported [2]. Concentrations of representative liver enzymes, such as aspartate amino transferase and alanine transaminase, did not differ among the groups. Lower food intake, associated with lower glucose and insulin levels, suggested that the animals were starved. However, the plasma level of FFAs was decreased and that of TG increased, which is not consistent with a starved condition. Based on these observations, we sought to examine the hepatic metabolism in this model since the liver plays a key role in the homeostasis of systemic catabolism and anabolism.

3.3. Analysis of energy metabolic pathways in the liver

Liver weight corrected by body weight was increased in CHF rats compared with control rats (Fig. 4A). The increase in liver weight is likely to be due to congestion since venous dilation in liver tissue is reported in this model [12]. It is of interest that increased right atrial pressure is reported to indicate malnutrition in CHF patients [13]. Despite lower blood sugar levels, the uptake of ^{18}FDG increased in CHF rats (Fig. 4B). The uptake of ^{125}I-9MPA, a fatty acid analog, was not changed (Fig. 4B). The amount of glycogen in liver was decreased, and that of TG was increased in the CHF rats (Fig. 5A, B). The metabolome analysis (Supplementary table) revealed that levels of some metabolites of glycolysis increased (Fig. 6A) and some metabolites in the Krebs cycle, such as acetyl-CoA and citrate, were decreased (Fig. 6B). Overall, these results may suggest hepatic lipogenesis to be increased and acetyl-CoA to be used for the synthesis of TG and cholesterol.

Next, we examined the gene expression related to lipogenesis and gluconeogenesis. The gene expression of enzymes related to lipogenesis, such as ATP citrate lyase, acetyl-CoA carboxylase, and fatty acid synthase, was up-regulated in CHF rats (Fig. 7A). In contrast, the expression of rate-limiting enzymes in gluconeogenesis, such as pyruvate carboxylase and phosphoenolpyruvate carboxykinase (PEPCK), was down-regulated. Next, we examine the expression of sterol regulatory element-binding protein (SREBP1)1-c and SREBP2, which increase lipogenesis and suppress gluconeogenesis [14,15]. The gene expression of SREBP1-c and SREBP2 was increased in CHF rats. The amount of SERBP proteins was also increased (Fig. 7B and C).

3.4. Expression of rapid turnover protein in liver

Since RBP, a blood hepatic protein, was decreased in the blood of CHF rats, we examined the gene expression of serum hepatic proteins. mRNA levels of transthyretin and retinol-binding protein (RBP) 4 were decreased in CHF rats (Fig. 8A). To examine the mechanism responsible for the decrease of rapid turnover proteins, we measured the expression of hepatocyte nuclear factor (HNF) 4. HNF4 is known to regulate transthyretin gene expression [16,17]. HNF4 mRNA levels started to decrease in rats with HT, and decreased significantly in rats with CHF (Fig. 8B).

3.5. Expression of proinflammatory genes

Inflammatory responses are reported to enhance lipogenesis [18] and induce cachexia [19]. It is well established that CHF is associated with the inflammation of cardiac and extra-cardiac tissue [20]. Thus, local inflammatory responses might be a mechanism causing

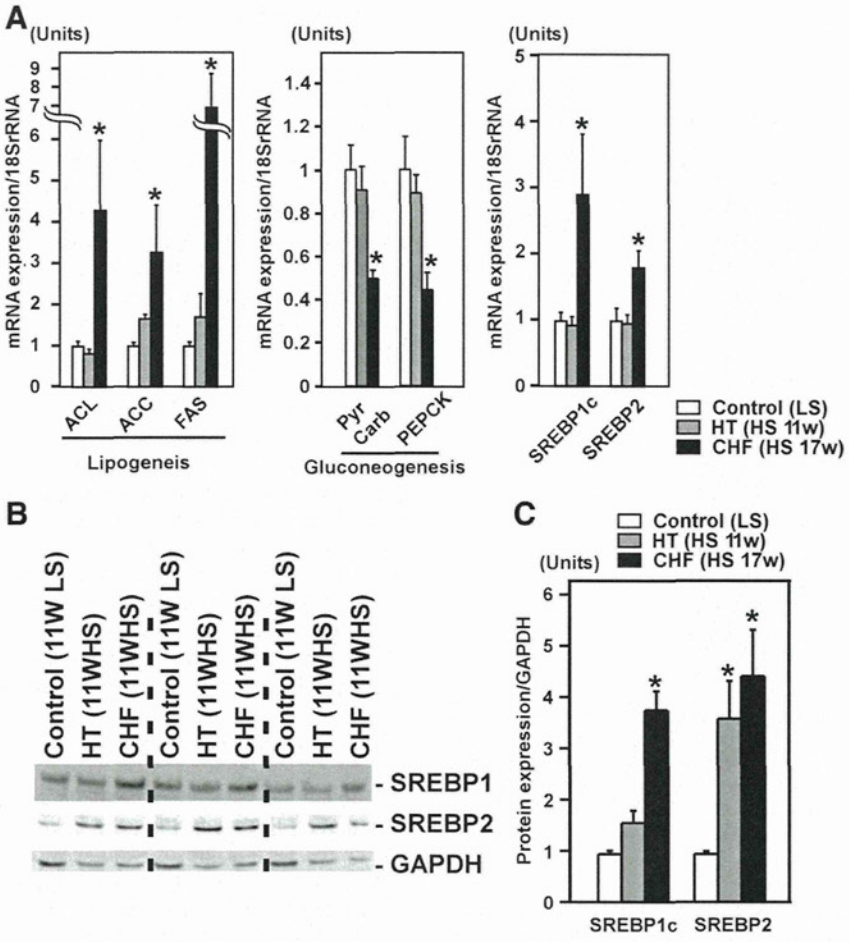

Fig. 7. Expression of mRNA and protein levels related to lipogenesis and gluconeogenesis. (A) The gene expression related to lipogenesis was increased in liver of CHF rats (HS 17W). The gene expression related to gluconeogenesis was decreased. The gene expression of sterol regulatory element-binding protein (SREBP)1c and SREBP2 was increased. n = 6–8 in each group. *p<0.05 versus control rats. (B) Representative images of the Western blotting of SREBP1 and SREBP2. (C) The protein levels of SREBP1 and SREBP2 in liver tissue were increased. n = 3 in each group. LS; low salt, HS; high salt. *p<0.05 versus control rats.

increased lipogenesis and the decreased synthesis of blood hepatic proteins. Therefore, we examined the expression of genes related to proinflammatory responses. The gene expression of TNF-α, IL1-β, and C-reactive protein, started to increase in liver of rats with HT but not with CHF, and significantly increased in CHF (Fig. 9A). The protein levels of TNF-α and interleukin1-β in liver also started to increase in HT rats, and remained increased in CHF rats (Fig. 9B).

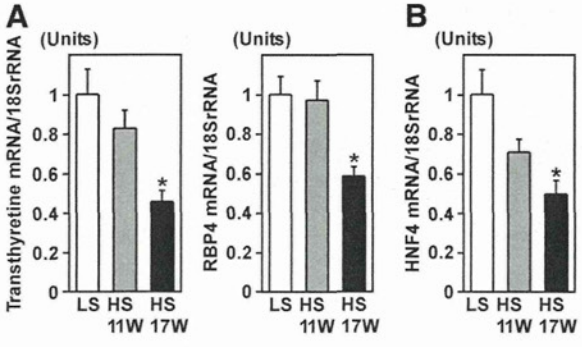

Fig. 8. Analysis of gene expression of hepatic proteins. (A) The gene expression of hepatic proteins, transthyretin and RBP4, was decreased in CHF rats (HS 17W). (B) Hepatocyte nuclear factor (HNF) 4 mRNA was decreased in CHF rats. n = 6–8 in each group. LS; low salt, HS; high salt. *p<0.05 versus control rats.

4. Discussion

In this study, we have shown that Dahl rat fed a high-salt diet developed CHF associated with a failure to grow, decreased blood hepatic protein, and increased blood proinflammatory cytokines. These results indicate the Dahl rat with CHF to be a model of cardiac cachexia.

4.1. Abnormal lipid metabolism in liver of CHF rats

During fasting, liver metabolism changes from anabolism to catabolism. Glucose is produced from glycogen breakdown and gluconeogenesis, and lipid accumulated as TG is used to produce FFAs. The glucose and FFAs are released into the circulation and delivered to the brain, skeletal muscle, the heart etc. However, despite decreased food intake and lower blood sugar and insulin levels, lipogenesis was increased in the liver of CHF rats (Fig. 10). The mechanism by which lipogenesis is increased on fasting in these rats is unknown. However, Fon Tacer et al. reported that giving TNF-α to fasted mice changed the metabolic profile of the liver from lipid usage to synthesis [18]. In that report, SREBP levels were are decreased in fasted mice, but increased on addition of TNF-α, associated with increased lipogenesis. Another report also showed abnormal lipid metabolism to be associated with inflammatory responses in liver [21]. Indeed, SREBPs increased in association with the amount of TNF-α mRNA and protein in this study. The TNF-α concentration in

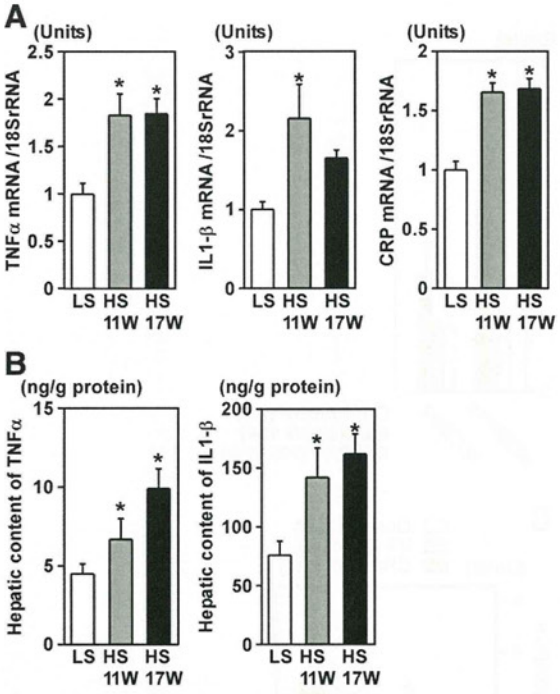

Fig. 9. Expression of proinflammatory cytokines in liver. (A) The gene expression of proinflammatory cytokines, TNF-α, IL1-β, and C-reactive protein (CRP), was increased in HT (HS 11W) and CHF rats (HS 17W). n = 6–8 in each group. (B) The amounts of TNF-α and IL1-β started to increase in the liver in HT rats, and remained increased in the liver in CHF rats assessed by ELISA. n = 6 in each group. LS; low salt, HS; high salt. *p<0.05 versus control rats.

liver was reported to be increased in an animal model of pacing-induced heart failure [22]. Thus, CHF-associated proinflammatory responses may be a mechanism of abnormal lipid metabolism in CHF rats.

4.2. Abnormal blood hepatic protein synthesis in CHF

Blood levels of hepatic proteins are used to evaluate nutritional status, but they are also influenced by many factors other factors. Particularly, the presence of inflammation is known to inversely correlate with circulating levels of hepatic proteins. Indeed, the gene expression of hepatic proteins was decreased associated with local increases in proinflammatory molecules of the liver in this study. However, the mechanism by which inflammation affects hepatic protein is not known [10]. HNF4 regulates the gene expression of transthyretin [16,17]. Although the mechanism by which proinflammatory molecules act on HNF4 expression is unclear, increased levels of SREBPs are known to repress HNF4 gene expression [23].

4.3. Measurement of metabolites using metabolome analysis

The measurement of metabolites in glycolysis and the Krebs cycle provides a snap shot of metabolism. However, based on the findings that ^{18}FDG uptake was increased, the amount of metabolites in glycolysis was increased, the amount of metabolites in the Krebs cycle was decreased, and the TG content was increased, we speculate that acetyl-CoA might be used for *de novo* lipogenesis. Further analysis, in which isotope-labeled glucose or fatty acid is injected and isotope-labeled metabolites are measured, is needed to know how glucose or fatty acids are used to test if the speculation is correct [24,25].

4.4. Potential role of abnormal liver metabolism in cardiac cachexia

Food intake was reduced and blood sugar levels were decreased in this model. During fasting, the liver is expected to deliver energy substrates, such as glucose and FFAs, to peripheral tissues. However, paradoxically, liver incorporated more glucose, the expression of genes related to gluconeogenesis was decreased, the expression of genes related to lipogenesis was increased, and TG content was increased. The response appears to be maladaptive, when the body is

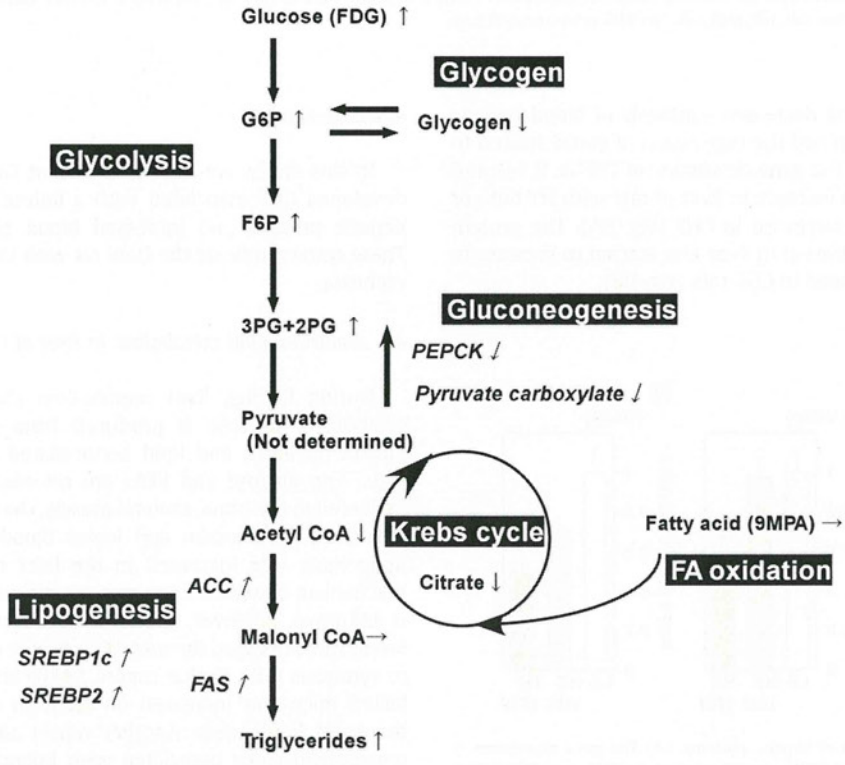

Fig. 10. Summary of the metabolic prolife in liver of CHF rats. Liver incorporated more glucose, gene expression related to gluconeogenesis was decreased, gene expression related to lipogenesis was increased, and TG content was increased in CHF rat liver.

losing weight and peripheral tissues need more substrates to maintain tissue homeostasis. Although this study is an observational one, the findings indicate the abnormal liver metabolism to be a maladaptive process and worsen the CHF. Further study of whether the modulation of liver metabolism ameliorates CHF is needed.

Acknowledgements

The authors of this manuscript have certified that they comply with the Principles of Ethical Publishing in the International Journal of Cardiology [30].

Appendix A. Supplementary data

Supplementary data to this article can be found online at doi:10.1016/j.ijcard.2011.07.056.

References

[1] Neubauer S. The failing heart — an engine out of fuel. N Engl J Med 2007;356:1140–51.
[2] Kato T, Niizuma S, Inuzuka Y, et al. Analysis of metabolic remodeling in compensated left ventricular hypertrophy and heart failure. Circ Heart Fail 2010;3:420–30.
[3] Doehner W, Rauchhaus M, Ponikowski P, et al. Impaired insulin sensitivity as an independent risk factor for mortality in patients with stable chronic heart failure. J Am Coll Cardiol 2005;46:1019–26.
[4] Anker SD, Sharma R. The syndrome of cardiac cachexia. Int J Cardiol 2002;85:51–66.
[5] Simonini A, Long CS, Dudley GA, et al. Heart failure in rats causes changes in skeletal muscle morphology and gene expression that are not explained by reduced activity. Circ Res 1996;79:128–36.
[6] Soga T, Ohashi Y, Ueno Y, Naraoka H, Tomita M, Nishioka T. Quantitative metabolome analysis using capillary electrophoresis mass spectrometry. J Proteome Res 2003;2:488–94.
[7] Rigden DJ, Jellyman AE, Frayn KN, Coppack SW. Human adipose tissue glycogen levels and responses to carbohydrate feeding. Eur J Clin Nutr 1990;44:689–92.
[8] Folch J, Lees M, Stanley GHS. A simple method for the isolation and purification of total lipids from animal tissues. J Biol Chem 1957;226:497–509.
[9] Shioi T, Kang PM, Douglas PS, et al. The conserved phosphoinositide 3-kinase pathway determines heart size in mice. EMBO J 2000;19:2537–48.
[10] Furman MP, Charney P, Mueller CM. Hepatic proteins and nutrition assessment. J Am Diet Assoc 2004;104:1258–64.
[11] Bernstein LH, Ingenbleek Y. Transthyretin: its response to malnutrition and stress injury. Clinical usefulness and economic implications. Clin Chem Lab Med 2002;40:1344–8.
[12] Inoko M, Kihara Y, Morii I, Fujiwara H, Sasayama S. Transition from compensatory hypertrophy to dilated, failing left ventricles in Dahl salt-sensitive rats. Am J Physiol 1994;267:H2471–82.
[13] Carr JG, Stevenson LW, Walden JA, Heber D. Prevalence and haemodynamic correlates of malnutrition in severe congestive heart failure secondary to ischaemic or idiopathic dilated cardiomyopathy. Am J Cardiol 1989;63:709–13.
[14] Shimano H. SREBPs: physiology and pathophysiology of the SREBP family. FEBS J 2009;276:616–21.
[15] Raghow R, Yellaturu C, Deng X, Park EA, Elam MB. SREBPs: the crossroads of physiological and pathological lipid homeostasis. Trends Endocrinol Metab 2008;19:65–73.
[16] Costa RH, Grayson DR. Site-directed mutagenesis of hepatocyte nuclear factor (HNF) binding sites in the mouse transthyretin (TTR) promoter reveal synergistic interactions with its enhancer region. Nucleic Acids Res 1991;19:4139–45.
[17] Wang Z, Burke PA. Hepatocyte nuclear factor-4α interacts with other hepatocyte nuclear factors in regulating transthyretin gene expression. FEBS J 2010;277:4066–75.
[18] Fon Tacer K, Kuzman D, Seliskar M, Pompon D, Rozman D. TNF-alpha interferes with lipid homeostasis and activates acute and proatherogenic processes. Physiol Genomics 2007;31:216–27.
[19] Sharma R, Anker SD. Cytokines, apoptosis and cachexia: the potential for TNF antagonism. Int J Cardiol 2002;85:161–71.
[20] Yndestad A, Damås JK, Oie E, Ueland T, Gullestad L, Aukrust P. Systemic inflammation in heart failure — the whys and wherefores. Heart Fail Rev 2006;11:83–92.
[21] Kleemann R, Verschuren L, van Erk MJ, et al. Atherosclerosis and liver inflammation induced by increased dietary cholesterol intake: a combined transcriptomics and metabolomics analysis. Genome Biol 2007;8:R200.
[22] Aker SD, Belosjorow S, Konietzka I, et al. Serum but not myocardial TNF-alpha concentration is increased in pacing-induced heart failure in rabbits. Am J Physiol Regul Integr Comp Physiol 2003;285:R463–9.
[23] Xie X, Liao H, Dang H, et al. Down-regulation of hepatic HNF4alpha gene expression during hyperinsulinemia via SREBPs. Mol Endocrinol 2009;23:434–43.
[24] Patel AB, de Graaf RA, Mason GF, Rothman DL, Shulman RG, Behar KL. The contribution of GABA to glutamate/glutamine cycling and energy metabolism in the rat cortex in vivo. Proc Natl Acad Sci USA 2005;102:5588–93.
[25] Metallo CM, Walther JL, Stephanopoulos G. Evaluation of ^{13}C isotopic tracers for metabolic flux analysis in mammalian cells. J Biotechnol 2009;144:167–74.
[26] Rodgers JT, Lerin C, Haas W, Gygi SP, Spiegelman BM, Puigserver P. Nutrient control of glucose homeostasis through a complex of PGC-1 and SIRT1. Nature 2005;434:113–8.
[27] Nadler EP, Dickinson EC, Beer-Stolz D, et al. Scavenging nitric oxide reduces hepatocellular injury after endotoxin challenge. Am J Physiol Gastrointest Liver Physiol 2001;281:G173–81.
[28] Puskás LG, Kitajka K, Nyakas C, Barcelo-Coblijn G, Farkas T. Short-term administration of omega 3 fatty acids from fish oil results in increased transthyretin transcription in old rat hippocampus. Proc Natl Acad Sci USA 2003;100:1580–5.
[29] Li J, Tao R, Wu W, et al. Transcriptional profiling and hepatogenic potential of acute hepatic failure-derived bone marrow mesenchymal stem cells. Differentiation 2010;80:166–74.
[30] Shewan LG, Coats AJ. Ethics in the authorship and publishing of scientific articles. Int J Cardiol 2010;144:1–2.